JATIS Journal of Astronomical Telescopes, Instruments, and Systems

RESEARCH PAPER

Solar system science with the Single Aperture Large Telescope for Universe Studies space observatory

Carrie M. Anderson,[a,*] **Nicolas Biver**,[b] **Gordon L. Bjoraker**,[a] **Thibault Cavalié**,[b,c] **Gordon Chin**,[a] **Michael A. DiSanti**,[a] **Paul Hartogh**,[d] **Nathan X. Roth**,[e,f] **Alexander Tielens**,[g] **and Christopher K. Walker**[h]

[a]NASA Goddard Space Flight Center, Planetary Systems Laboratory, Greenbelt, Maryland, United States
[b]Sorbonne Université, Université Paris-Cité, Université PSL, CNRS, LESIA, Observatoire de Paris, Meudon, France
[c]University of Bordeaux, CNRS, Laboratoire d'Astrophysique de Bordeaux, Pessac, France
[d]Max Planck Institute for Solar System Research, Göttingen, Germany
[e]American University, Department of Physics, Washington, District of Colombia, United States
[f]NASA Goddard Space Flight Center, Astrochemistry Laboratory, Greenbelt, Maryland, United States
[g]University of Maryland, Astronomy Department, College Park, Maryland, United States
[h]University of Arizona, Department of Astronomy and Steward Observatory, Tucson, Arizona, United States

ABSTRACT. Single Aperture Large Telescope for Universe Studies (SALTUS) is a NASA Astrophysics Probe Explorer (APEX)-class mission concept employing a robust far-infrared pointed space observatory. SALTUS comprises a 14-m inflatable reflector that provides 16× the sensitivity and 4× the angular resolution of Herschel, with a sunshield that radiatively cools the primary to 45 K, along with cryogenic detectors that collectively span the 34 to 660 μm far-infrared spectral range at high and moderate spectral resolutions. The high sensitivity and high spectral resolving power of the SALTUS heterodyne receivers enable both submillimeter and far-infrared observations of trace compounds comprising water and its isotopologues, hydrogen deuteride (HD), and a plethora of molecular species containing carbon, hydrogen, nitrogen, oxygen, phosphorus, or sulfur (CHNOPS), all of which are obscured by the Earth's atmosphere. The high sensitivity and broadband spectral coverage of the SALTUS far-infrared grating spectrometer enables far-infrared observations of the lattice vibrational spectral signatures of ices and mineral grains contained within a wide variety of solar system targets, including comets, planetary atmospheres, near Enceladus' plumes, and on the surfaces of icy moons, Jupiter trojans, centaurs, and Kuiper Belt objects. A key objective of SALTUS is to measure HDO/H_2O in both Jupiter family and Oort cloud comets. Additional observations will allow us to characterize the water torus around Saturn generated by its icy moon Enceladus, determine the source of stratospheric water in the giant planets, ascertain the time evolution of water on Venus, and search for H_2O plumes on Europa, Ganymede, and Callisto. SALTUS will measure HD/H_2 in all four giant planets to constrain models of their origin. SALTUS can also measure the abundance of CHNOPS-containing molecules and halides in the atmosphere of Venus and in the comae of comets. We review the extensive amount of solar system science achievable with SALTUS for both the Guaranteed Time Observation and the Guest Observer APEX mission observing programs.

Keywords: solar system; astrochemistry; cosmic origins; terahertz spectroscopy; far-infrared; space telescopes

Paper 24016SS received Mar. 6, 2024; revised Jun. 7, 2024; accepted Jul. 12, 2024; published Sep. 4, 2024.

*Address all correspondence to Carrie M. Anderson, carrie.m.anderson@nasa.gov

1 Introduction

Single Aperture Large Telescope for Universe Studies (SALTUS) is a robust, far-infrared (far-IR) pointed space observatory concept that was responsive to NASA's Astrophysics Probe Explorer (APEX) Announcement of Opportunity (AO) in November 2023. If selected, the phase-E science operations portion of the SALTUS mission will commence in 2032, with a 5-year baseline mission. During these 5 years, SALTUS will observe thousands of astrophysical targets, including galaxies, protoplanetary and debris disks, and a significant number of solar system objects; all of these targets fall within key science areas raised in the Astrophysics Decadal Survey, *Pathways to Discovery in Astronomy and Astrophysics for the 2020s*[1] (Astro2020), and in the Astrophysics Roadmap, *Enduring Quests and Daring Visions*[2] (see Sec. 1.1). Without a dedicated space observatory that operates at long wavelengths in the far-IR regime, coupled with high-sensitivity and high-spectral resolving power instruments, the low-energy transitions of hydrogen deuteride (HD), water and its isotopologues [$H_2{}^{16}O$, singly deuterated water (HDO), $H_2{}^{17}O$, $H_2{}^{18}O$], a profusion of molecules containing carbon, hydrogen, nitrogen, oxygen, phosphorus, or sulfur (CHNOPS), and lattice vibrational modes of astrophysically relevant ices and minerals cannot be measured. This is due to Earth's strongly absorbing troposphere (Fig. 1), where many of such molecules in the far-IR reside and are therefore inaccessible to ground-based telescopes, such as

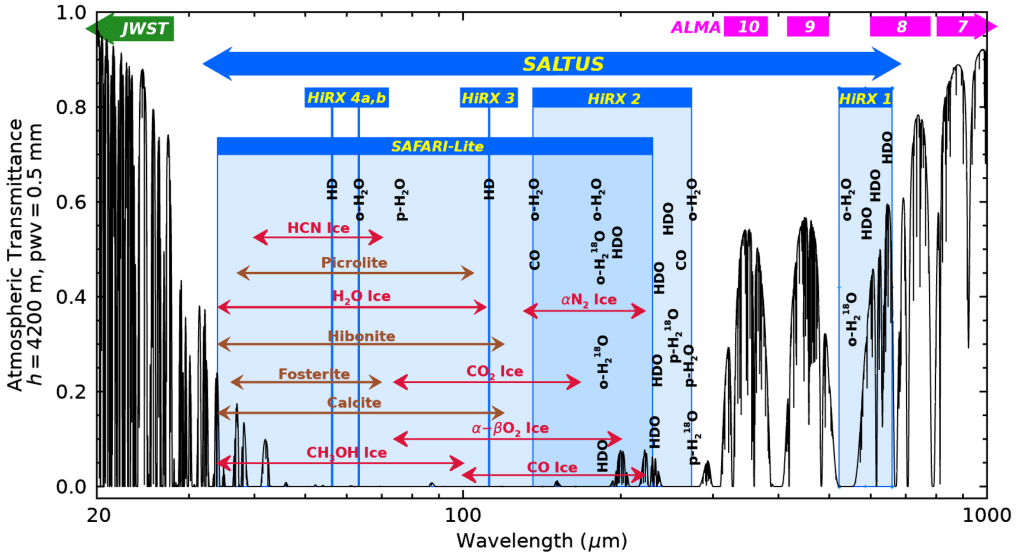

Fig. 1 Simulated terrestrial atmospheric transmission spectrum (black curve; radiative transfer model from Ref. 3) demonstrating the SALTUS far-IR spectral region that is inaccessible from the ground and outside of the operational wavelengths of JWST (green) and ALMA (magenta). The full spectral range of the SAFARI-Lite spectrometer spanning wavelengths 34 to 230 μm is indicated by the blue color-coded rectangle under the SAFARI-Lite heading, as is the HiRX instrument's tunable bands 1 to 4, with the full spectral range in tunability of each band indicated by the blue color-coded rectangles under the HiRX bands 1 to 4 headings. The spectral ranges encompassed by HiRX and SAFARI-Lite target critically important wavelengths that are significantly or completely blocked from the ground. This includes low-energy transitions of H_2O and its isotopologues and other important species such as the HD 1-0 and HD 2-1 transitions (the names of key molecules at their peak wavelength positions are superimposed in black), along with the spectral ranges of the low-energy lattice vibrational modes of many astrophysically relevant ices (identified in red) and minerals (identified in brown). Important transitions of key H_2O (ortho and para) and HDO lines and representative CO lines are provided, although HiRX can measure all intervening transitions. Moreover, SAFARI-Lite will be able to measure all lines in the 34 to 230 μm range, e.g., all CO lines starting at 13 to 12, including the accessible ^{13}CO lines, along with numerous ices such as water ice, αN_2 ice, and $\alpha - \beta O_2$ ice. SALTUS is designed to observe simultaneously in all four HiRX bands or the full spectral range of SAFARI-Lite, thus maximizing science return. The four HiRX bands use heterodyne technology providing $R = 10^5$ to 10^7 spectral resolving power, and SAFARI-Lite is a four-band grating spectrometer achieving continuous coverage from 34 to 230 μm with $R = 300$ spectral resolving power.

the Atacama Large Millimeter/submillimeter Array (ALMA). These far-IR transitions are also inaccessible to the James Webb Space Telescope (JWST) because they spectrally reside at $\lambda > 28$ μm. Space-borne observations at these long far-IR wavelengths are therefore essential.

SALTUS employs a 14-m off-axis primary aperture enabled by an innovative, lightweight, and inflatable telescope technology, with a sunshield that allows radiative cooling of the primary to a temperature of 45 K. The SALTUS observatory's technical details are given in Arenberg et al., "Design, Implementation and Performance of the Primary Reflector for SALTUS"; Kim et al., "SALTUS Observatory Optical Design and Performance"; and Harding et al., "SALTUS Probe Class Space Mission: Observatory Architecture & Mission Design," *J. Astron. Telesc. Instrum. Syst.* (this issue). The large telescope collecting area, in combination with the highly sensitive cryogenic instruments at high and moderate spectral resolutions, yields unprecedented high-spatial resolution measurements at the long, critically needed far-IR wavelengths (Sec. 2), making SALTUS a powerful tool for pointed observations. The two SALTUS cryogenic instruments are the high-resolution receiver (HiRX) and the grating spectrometer SAltus FAR-infrared Instrument (SAFARI)-Lite. HiRX comprises bands 1, 2, 3, 4a, and 4b, spanning wavelength ranges of 521.4 to 658.9, 136.3 to 272.5, 104.3 to 121.1, 62.7 to 63.7, and 55.8 to 56.7 μm, respectively. The four HiRX bands operate in parallel with one another, and to achieve measurements across the full spectral range of each band, the HiRX bands must be individually tuned in narrow frequency intervals. At the central wavelength of each band, the instantaneous bandwidths yield 750 MHz and 4 GHz for HiRX 1, using the fast fourier transform (FFT) and autocorrelation spectrometers, respectively, and 3.5 GHz for HiRX bands 2 to 4b, which solely use the autocorrelation spectrometer. Band 1 has spectral resolving powers $R = 1 \times 10^7$ and $R = 1 \times 10^5$ for the FFT and autocorrelation spectrometers, respectively, whereas bands 2 to 4b have resolving powers $R = 3 \times 10^5$ (band 2), $R = 5 \times 10^5$ (band 3), and $R = 1 \times 10^6$ (bands 4a, b). The system noise temperatures are 124 K (band 1), 484 K (band 2), 802 K (band 3), and 1555 K (bands 4a,b). The angular resolution at the center of each band is 10.3″, 2.9″, 2.0″, 1.1″, and 1.0″ for bands 1 to 4b, respectively. The HiRX instrument's technical details are given in Silva et al., "The High Resolution Receiver (HiRX) for the Single Aperture Large Telescope for Universe Studies (SALTUS)," *J. Astron. Telesc. Instrum. Syst.* (this issue).

The SAFARI-Lite grating spectrometer comprises short-wavelength (SW), medium-wavelength (MW), long-wavelength (LW), and very long-wavelength (VLW) bands, which have broadband coverage across the wavelength ranges 34 to 56, 54 to 89, 87 to 143, and 140 to 230 μm, respectively, with angular resolutions at the band centers of 0.66″ (SW), 1.1″ (MW), 1.7″ (LW), and 2.7″ (VLW). The instantaneous bandwidths of the four SAFARI-Lite bands are the full spectral range of each band. As with HiRX, the four SAFARI-Lite bands operate in parallel with one another, allowing for instantaneous coverage of the full 34 to 230 μm far-IR domain in a single observing session. Combined with the uniquely large SALTUS telescope, SAFARI-Lite will bring a significant improvement in spectral line sensitivity, surpassing by far any past or currently planned mission. With a spectral resolving power of 300, the current best estimate for the line intensity detection limit is on the order of 2×10^{-20} W/m^2 (5σ/1 h) with the advantage of not having to push detector sensitivity to the limit. The noise equivalent power requirement is $\sim 10^{-18}$ W/$\sqrt{\text{Hz}}$ (limited by the background signal), which is modest for the state-of-the-art kinetic inductance detectors. For technical details, see Roelfsema et al., "The SAFARI-Lite Imaging Spectrometer for the SALTUS Space Observatory," *J. Astron. Telesc. Instrum. Syst.* (this issue).

An overview of the HiRX and SAFARI-Lite instrument characteristics is given in Table 1. The spectral range, instantaneous bandwidth, and spectral resolving power for each band are given in wavelength, wavenumber, and frequency space, in respective units of μm, cm^{-1}, and GHz. The instantaneous bandwidths, spectral resolving powers, and angular resolutions provided reflect the central wavelength, wavenumber, or frequency of the given band spectral range. The 5σ sensitivity values integrated over 1 h are provided in mK units for HiRX and W/m^2 units for SAFARI-Lite. The spectral ranges of the HiRX and SAFARI-Lite bands are further illustrated in Figs. 1 and 2.

The APEX AO mandated that >70% of the SALTUS telescope allocation time resides within the NASA-managed Guest Observer (GO) program, where it is expected that a telescope allocation committee will review observing proposals, in a similar fashion to what routinely

Table 1 SALTUS instrument overview.

Band		No. of pixels	λ (μm) ν (cm^{-1}) f (GHz) Spectral range		Inst. BW	Spectral resolving power	Sensitivity (5σ, 1 h)	Ang. Res. ($''$)
HiRX	1 (FFT)	1	λ	658.9 to 521.4	0.86	1×10^{7}	18 mK	10.3
			ν	15.2 to 19.2	0.03			
			f	455 to 575	0.75			
	1 (ACS)	1	λ	658.9 to 521.4	4.58	1×10^{5}	18 mK	10.3
			ν	15.2 to 19.2	0.13			
			f	455 to 575	4.0			
	2	1	λ	272.5 to 136.3	0.43	3×10^{5}	63 mK	2.9
			ν	36.7 to 73.4	0.12			
			f	1100 to 2200	3.5			
	3	1	λ	121.1 to 104.3	0.15	5×10^{5}	671 mK	2.0
			ν	82.6 to 95.9	0.12			
			f	2475 to 2875	3.5			
	4a	7	λ	63.7 to 62.7	0.05	1×10^{6}	95 mK	1.1
			ν	156.9 to 159.6	0.12			
			f	4704 to 4784	3.5			
	4b	7	λ	56.7 to 55.8	0.04	1×10^{6}	95 mK	1.0
			ν	176.5 to 179.1	0.12			
			f	5290 to 5370	3.5			
SAFARI-Lite	VLW	180×6	λ	230 to 140	90	300	2×10^{-20} W/m^2	2.7
			ν	43.5 to 71.4	28			
	LW	180×6	λ	143 to 87	56	300	2×10^{-20} W/m^2	1.7
			ν	69.9 to 114.9	45			
	MW	180×6	λ	89 to 54	35	300	1×10^{-20} W/m^2	1.1
			ν	112.4 to 185.2	73			
	SW	180×6	λ	56 to 34	22	300	5×10^{-21} W/m^2	0.66
			ν	178.6 to 294.1	116			

FFT, fast fourier transform spectrometer; ACS, autocorrelation spectrometer; λ, wavelength in μm; ν, wavenumber in cm^{-1}; f, frequency in GHz; Inst. BW, instantaneous bandwidth; Ang. Res., angular resolution

occurs with space- and ground- based observatories (e.g., Hubble Space Telescope, JWST, ALMA, and the W. M. Keck observatory). The remaining telescope time (<30%) is allotted for the SALTUS science co-investigators as part of the Guaranteed Time Observation (GTO) program. However, with the SALTUS observatory's operational efficiency of ~80%, the breakdown between GO and GTO allocation times is closer to an 80/20 split, as detailed in the SALTUS observatory's overview paper by Chin et al., "Single Aperture Large Telescope for Universe

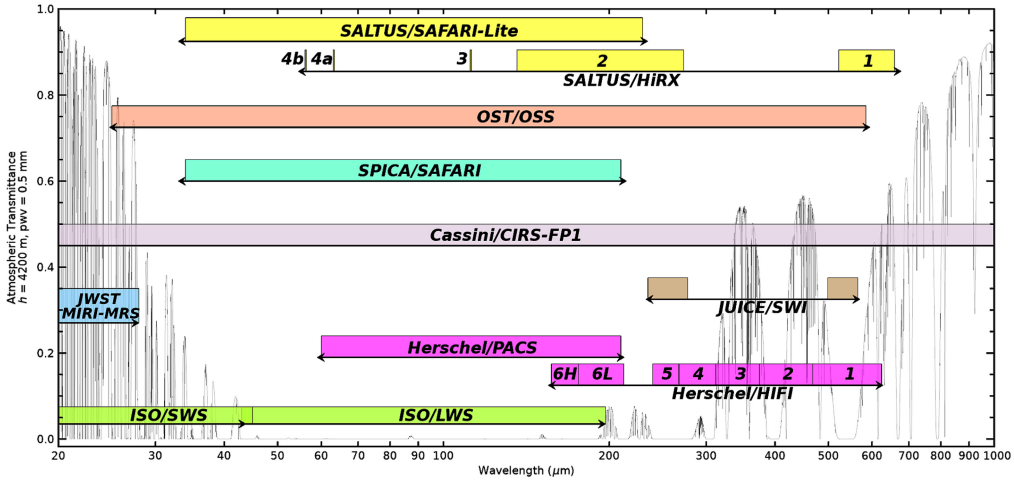

Fig. 2 Spectral ranges covered by far-IR space observatory mission concepts, far-IR space observatories that have flown, and far-IR planetary flight spacecraft that have flown. Superimposed (in black) is the simulated transmittance spectrum of the Earth's atmosphere, as depicted in Fig. 1. Mission concepts are indicated in yellow, light coral, and aqua, respectively, for the SALTUS HiRX and SAFARI-Lite instruments, the Origin Space Telescope's OSS instrument, and the SPace Infrared telescope for Cosmology and Astrophysics SAFARI instrument. Far-IR space observatories that have flown are shown in lime green, sky blue, and magenta for ISO's SWS and LWS instruments, the longest wavelength JWST instrument (MIRI-MRS), and Herschel's PACS and HIFI instruments, respectively. Finally, far-IR flight instruments onboard planetary flight spacecraft that have flown are given in lilac and tan respectively representing Cassini's CIRS instrument (FP1 interferometer) and JUICE's SWI instrument.

Studies (SALTUS): Probe Mission and Science Overview," *J. Astron. Telesc. Instrum. Syst.* (this issue). Tables 2–5 identify which solar system science observing agendas (science details given in Sec. 2) are designated GO or GTO and describe the impact of the SALTUS measurements, whether part of the threshold or baseline science agendas (Sec. 2.1). It should be noted that all GO science themes presented in Sec. 2 are illustrative GO, in that they are representative of a long list of potential GO topics that the science community might propose based on the science themes given in Astro2020.[1] As per the AO requirement, all SALTUS data, regardless of GO or GTO observing program, will be made publicly available within 6 months via a NASA-managed astrophysics data archive (e.g., Infrared Processing and Analysis Center).

Table 2 SALTUS Solar System Science theme 1.

Science theme 1: Trace the origin and history of water delivered to the solar system by observing the isotopologues in comets, ocean world and planetary atmospheres, and other known water reservoirs		
Threshold	GTO	Measurement of at least five transitions of HDO in six to eight comets (both Jupiter Family and Oort Cloud comets) with HiRX 1 and 2; characterization of Saturn's water torus generated by Enceladus and detection of Europa's H_2O plumes at 538.3 μm with HiRX 1
	GO	Measurement of water in the giant planet stratospheres with HiRX 2; detection of Ceres' water atmosphere at 538.3 μm with HiRX 1
Baseline	GTO	Extension of the number of HDO/H_2O measurements in comets by a factor of 5 to 30 to 40 comets with HiRX 1 and 2
		Spatial maps of Enceladus' H_2O and repeated observations for different orbital positions at Europa, Ganymede, and Callisto with HiRX 1 and 2, using the 538.3 and 179.5 μm transitions, $H_2{}^{18}O$ transitions, and other species such as CO
	GO	Spatial maps of additional H_2O transitions and their corresponding isotopologues in the giant planet stratospheres and the atmospheres of Ceres, Venus, Titan, Triton, and Pluto with HiRX 1 and 2

Table 3 SALTUS Solar System Science theme 2.

Science theme 2: Measure the D/H ratios in HD in the giant planets to constrain their formation		
Threshold	GTO	Detection of two HD transitions in the giant planet upper tropospheres and stratospheres with HiRX 3 and HiRX 4b
Baseline	GTO	Spatial maps with HiRX 3 and the HiRX 4b array of two HD transitions on Jupiter and Saturn, along with CH_4, to determine whether D/H varies with latitude. If not, then HD serves as another thermometer that probes deeper than CH_4

Table 4 SALTUS Solar System Science theme 3.

Science theme 3: Investigate the role of particulates contained within comets, planetary atmospheres, and near Enceladus' plumes and on the surfaces of icy moons, Jupiter trojans, centaurs, and Kuiper belt objects (KBOs)		
Threshold	GTO	Observational demonstration using SAFARI-Lite in year 1 of H_2O ice in four to six comets and Enceladus' plumes and organic ices in Titan's stratosphere
	GO	Detection of far-IR spectral signatures of silicates and ices in Jupiter trojans and KBOs with SAFARI-Lite
Baseline	GTO	Spectral surveys in years 2 to 5 using the full range of SAFARI-Lite targeting pure and mixed CO, CO_2, N_2, O_2, and H_2O ice in 30 to 40 comets, CH_4 ice in the giant planet stratospheres, organic ices in Titan's stratosphere, and water ice within 2″ of Enceladus' plumes
	GO	Spectral surveys using the full spectral range of SAFARI-Lite targeting the threshold mission-detected ices, organic compounds, and silicates in Jupiter trojans, centaurs, KBOs, and the surfaces of the Galilean moons and Triton

Table 5 SALTUS Solar System Science theme 4.

Science theme 4: Measure the abundances of CHNOPS-containing molecules and halides in the atmospheres of Venus and comets		
Threshold	GO	Detection of spectral signatures of astrochemically relevant compounds in Venus' middle atmosphere with HiRX 1 and 2
Baseline	GO	Spectral surveys using the full spectral range of HiRX 1 and 2 targeting the threshold mission-detected astrochemically relevant compounds in 30 to 40 comets and in Venus' middle/upper atmosphere

1.1 Programmatic Motivation

SALTUS Solar System Science will answer fundamental, high-priority science questions raised in Astro2020,[1] the NASA Astrophysics Roadmap,[2] the NASA 2022 Strategic Plan, and the NASA 2020 Science Plan, which are all expanded below:

1. Astro2020[1]
   - 1.1. Question E-Q2b: How does a planet's interior structure and composition connect to its surface and atmosphere? SALTUS will address this question by measuring the D/H ratios in HD in the upper tropospheres and stratospheres of the giant planets to constrain their formation, which aids in significantly improving giant planet formation models (Sec. 2.3).
   - 1.2. Question E-Q2c: What fundamental planetary processes determine the complexity of planetary atmospheres? SALTUS will address this question by investigating the ongoing processes occurring within atmospheres, such as photochemistry, cloud formation, and atmospheric dynamics, thereby providing a clearer understanding of the evolutionary pathways of the planets within our own solar system, which can then be used to compare with exoplanetary systems (Secs. 2.2, 2.4, and 2.5).

Table 6 Spatial resolution comparisons.

Observatory spatial resolution (″)			Target angular size/observatory spatial resolution							
			Venus	Jupiter	Europa	Saturn	Titan	Enceladus	Uranus	Neptune
160 μm	ISO LWS	67.1	0.98	0.75	0.02	0.30	0.01	0.001	0.06	0.04
	Herschel PACS	11.5	5.74	4.35	0.09	1.74	0.07	0.006	0.32	0.21
	SALTUS S-L	2.9	22.76	17.24	0.35	6.90	0.28	0.02	1.28	0.83
560 μm	Herschel HIFI	40.3	1.64	1.24	0.03	0.50	0.02	0.002	0.09	0.06
	SALTUS HiRX	10.1	6.53	4.95	0.10	1.98	0.08	0.007	0.37	0.24

1.3. Questions E-Q3a,b: How are potentially habitable environments formed? What processes influence the habitability of environments? SALTUS will address these questions by tracing the inventory and history of volatiles and organics within a diverse range of planetary and cometary atmospheric environments. These measurements also allow for Venus to be used as ground truth for terrestrial exoplanet analogs (Secs. 2.2 and 2.5).

2. the Astrophysics Roadmap, NASA Astrophysics in the Next Three Decades,[2] which promotes investigations of giant planets, terrestrial planets, and ocean worlds.
3. the NASA 2022 Strategic Plan, in which SALTUS's Science Objective 2 addresses NASA's broad strategic goal of exploring the question, How did we get here?
4. the 2020 Science Plan, Science 2020–2024: a Vision for Scientific Excellence, FY21–22 Update, in which the SALTUS mission falls within NASA Strategies 1.2 and 1.3.

SALTUS solar system observations will expand upon the pioneering far-IR measurements acquired by Herschel's photodetector array camera and spectrometer (PACS) and heterodyne instrument for the far-infrared (HIFI) instruments, the Infrared Space Observatory's (ISO) long-wavelength spectrometer (LWS) instrument, and Cassini's composite infrared spectrometer (CIRS) instrument. Examples of the science synergies between SALTUS and these former far-IR telescopes are provided in Secs. 2.2.2, 2.3, 2.4, and 2.4.5, and Fig. 2 compares the spectral coverage between SALTUS and these far-IR space observatories, flight missions, and mission concepts. In addition, Table 6 provides the spatial resolution between SALTUS, Herschel, and ISO at 160 and 560 μm, and the ratios between the angular diameters of eight solar system objects (Venus, Jupiter, Europa, Saturn, Enceladus, Titan, Uranus, and Neptune) with the observatory spatial resolutions at 160 and 560 μm. These comparisons directly reveal if a target is resolved, demonstrating that even if unresolved, the beam dilution factor when observing with SALTUS is significantly less than occurs with Herschel and ISO, which affects integration time and, ultimately, signal-to-noise ratios. SALTUS Solar System Science also resonates with the science drivers encompassing many ongoing missions, future missions, and mission concepts, such as:

i. NASA's Venus Emissivity, Radio Science, InSAR, Topography, and Spectroscopy (VERITAS) discovery mission to Venus
ii. NASA's Deep Atmosphere Venus Investigation of Noble gases, Chemistry, and Imaging (DAVINCI) discovery mission to Venus
iii. ESA's EnVision, an orbital mission concept to Venus

iv. ESA's Jupiter Icy Moons Explorer (JUICE) mission, an orbital mission en route to the Jupiter System
v. NASA's Juno mission, an orbital mission in the Jupiter system
vi. NASA's Europa Clipper mission
vii. NASA's Dragonfly mission to Titan
viii. NASA's New Frontiers 5 to 7 mission opportunities to comets, Io, Enceladus, and Saturn
ix. ESA's L4 mission opportunity to moons of the giant planets
x. NASA's Uranus and Enceladus future Flagship mission opportunities
xi. NASA's JWST Space Observatory
xii. NASA's future Habitable World Space Observatory (HWO).

2 Solar System Science with SALTUS

The high spectral resolution, high spatial resolution, high sensitivity, and broad spectral coverage of SALTUS at far-IR wavelengths are made possible due to a unique combination of its large aperture and its two cryogenic instruments, HiRX and SAFARI-Lite. The SALTUS inflatable reflector provides 16× the sensitivity and 4× the angular resolution of the Herschel Space Observatory, in which the former reduces required observing times by a factor of 256 per measurement, thereby enabling the detection of far-IR transitions of water and other molecules within minutes. The SALTUS large aperture further enables unprecedented high spatial resolution at these long wavelengths, with example beam sizes of 9.7″ at 538.3 μm [$1_{10} \rightarrow 1_{01}$ ortho-H_2O; HiRX 1], 3.2″ at 179.5 μm [$2_{12} \rightarrow 1_{01}$ ortho-H_2O; HiRX 2], 2.0″ at 112.1 μm [$1 \rightarrow 0$ HD; HiRX 3], 1.0″ at 56.2 μm [$2 \rightarrow 1$ HD; HiRX 4b], and 0.61″ at 34 μm [shortest SAFARI-Lite wavelength], see also Table 6. Tables 7 and 8 highlight some of the key molecules available in the four HiRX bands, and Table 9 highlights some of the key ice and mineral signatures available in the four SAFARI-Lite bands. As a result, SALTUS brings significant capabilities to solar system science, which is critical to the SALTUS mission goal of exploring our cosmic origins and the possibility of life elsewhere. The unique capabilities of SALTUS allow for the characterization of astrochemical signatures from environments within the solar system, as well as the conditions for habitability that developed during its formation, which falls under SALTUS Science Objective 2: Probe the physical structure of protoplanetary disks and follow the trail of water and organics from protoplanetary disks to the solar system, from which the solar system portion can be further broken down into the following four science themes:

Science Theme 1: *Trace the origin and history of water delivered to the solar system by observing the isotopologues in comets, ocean worlds, planetary atmospheres, and other known water reservoirs.* This science theme incorporates both GO and GTO observing programs, which are expanded on in Table 2. An overview of this theme involves revealing the time evolution of the D/H ratio by measuring at least five distinct HDO lines in 30 to 40 comets over 5 years and conducting repeated observations of Enceladus' torus, Ganymede, Callisto, and Europa to map out the spatially varying H_2O abundances and to constrain the processes responsible for maintaining these ocean world atmospheres (see Sec. 2.2 for more details).

Science Theme 2: *Measure the D/H ratios in HD in the giant planets to constrain their formation.* This theme is solely GTO and is expanded on in Table 3. SALTUS will measure HD abundances in the tropospheres and stratospheres of the giant planets, which will significantly improve upon the accuracy of previous D/H estimates (see Sec. 2.3 for more details).

Science Theme 3: *Investigate the role of particulates contained within comets and planetary atmospheres, near Enceladus' plumes, and on the surfaces of icy moons, Jupiter trojans, centaurs, and Kuiper Belt objects (KBOs).* This theme comprises both GO and GTO observing programs, which are expanded on in Table 4. SALTUS will make measurements of solar system particulates that provide a powerful means to retrieve information on the chemical, physical, and evolutionary processes occurring within these vastly diverse environments (see Sec. 2.4 for more details).

Table 7 Example water transitions available with HiRX.

		Spectral peak			
Molecule	Transition	λ (μm)	ν (cm^{-1})	f (GHz)	HiRX band
o – $H_2^{16}O$	1_{10} to 1_{01}	538.30	18.58	556.92	1
	3_{12} to 3_{03}	273.19	36.60	1097.36	2
	2_{12} to 1_{01}	179.53	55.70	1669.90	
	3_{30} to 3_{21}	136.50	73.26	2196.34	
	2_{21} to 2_{12}	180.50	55.41	1661.0	
	3_{12} to 2_{21}	259.98	38.46	1153.12	
	3_{21} to 3_{12}	257.79	38.79	1162.93	
	3_{03} to 2_{12}	174.63	57.27	1716.76	
o – $H_2^{18}O$	1_{10} to 1_{01}	547.38	18.27	547.69	1
	3_{12} to 3_{03}	273.63	36.55	1095.62	2
	2_{12} to 1_{01}	181.05	55.23	1655.87	
	3_{03} to 2_{12}	174.37	57.35	1719.25	
	3_{30} to 3_{21}	139.84	71.51	2143.76	
	2_{21} to 2_{12}	183.53	54.49	1633.48	
o – $H_2^{17}O$	1_{10} to 1_{01}	543.10	18.41	552.01	1
	2_{12} to 1_{01}	180.33	55.45	1662.47	2
p – $H_2^{16}O$	1_{11} to 0_{00}	269.27	37.14	1113.34	2
	3_{22} to 3_{13}	156.19	64.02	1919.36	
	3_{13} to 2_{02}	138.53	72.19	2164.14	
	2_{20} to 2_{11}	243.97	40.99	1228.79	
	8_{18} to 7_{07}	63.32	157.92	4734.30	4a
p – $H_2^{18}O$	1_{11} to 0_{00}	272.12	36.75	1101.71	2
	2_{20} to 2_{11}	250.03	40.00	1199.02	
	3_{22} to 3_{13}	158.26	63.19	1894.33	
	3_{13} to 2_{02}	139.59	71.64	2147.74	
HDO	1_{01} to 0_{00}	644.83	15.51	464.92	1
	2_{02} to 1_{11}	611.06	16.37	490.61	
	1_{10} to 1_{01}	588.65	16.99	509.29	
	3_{21} to 3_{12}	246.29	40.60	1217.26	2
	2_{12} to 1_{01}	239.64	42.62	1277.69	
	2_{20} to 2_{11}	232.10	43.08	1291.64	
	3_{13} to 2_{12}	236.61	42.26	1267.04	
	2_{21} to 2_{12}	196.85	50.80	1522.93	
	3_{13} to 2_{02}	184.44	54.22	1625.41	

Table 8 Example non-water transitions available with HiRX.

Molec.	Spectral peak			HiRX band	Molec.	Spectral peak			HiRX band
	λ (μm)	ν (cm^{-1})	f (GHz)			λ (μm)	ν (cm^{-1})	f (GHz)	
HD	56.23	177.84	5331.55	4b	OCS	632.39	15.81	474.06	1
	112.07	89.23	2674.99	3		587.30	17.03	510.46	
^{12}CO	650.24	15.38	461.05	1	$OC^{34}S$	648.26	15.43	462.46	
	260.24	38.43	1151.98	2		632.07	15.82	474.30	
^{13}CO	544.16	18.38	550.93	1	$O^{13}CS$	651.13	15.36	460.42	
	272.21	36.74	1101.35	2	H_2S	187.40	53.36	1599.78	2
$C^{18}O$	248.44	40.25	1206.73			175.53	56.98	1707.98	
	182.30	54.86	1644.51		$H_2{}^{34}S$	250.53	39.92	1196.62	
	273.25	35.60	1097.15			176.84	56.87	1704.89	
CH_4	238.69	41.90	1255.98	2	$H_2{}^{33}S$	595.98	16.78	503.01	1
	238.68	41.90	1256.07			176.14	56.77	1702.01	2
	190.98	52.36	1569.74		SO_2	539.52	18.54	555.67	1
$^{13}CH_4$	238.68	41.90	1256.04			259.33	38.56	1156.03	2
	191.03	52.35	1569.32		$^{34}SO_2$	536.57	18.64	558.72	1
CH_3D	257.89	38.78	1162.48			267.07	37.44	1122.51	2
	184.33	54.25	1626.40		H_2O_2	254.35	39.32	1178.66	2
H_2CO	256.76	38.95	1167.60	2		181.46	55.11	1652.16	
	179.38	55.75	1671.25		HCl	239.91	41.68	1249.59	2
$H_2{}^{13}CO$	546.60	18.30	548.47	1		239.56	41.74	1251.45	
	258.73	38.65	1158.73	2	HCN	563.83	17.74	531.71	1
$H_2C^{18}O$	544.69	18.36	550.39			260.36	38.41	1151.44	2
	524.58	19.06	571.49		$H^{13}CN$	578.77	17.28	517.98	1
HCOOH	645.58	15.49	464.38	1		267.27	37.42	1121.70	2
	588.65	16.99	509.29		$HC^{15}N$	580.69	17.22	516.27	1
O_2	615.27	16.25	487.25	1		268.15	37.29	1117.99	2
	171.19	58.42	1751.27	2	NH_3	523.67	19.10	572.48	1
$O^{18}O$	528.83	18.91	566.90	1		170.0	58.83	1763.53	2
	175.12	57.11	1711.98	2	$^{15}NH_3$	524.0	19.08	572.12	1
O_3	642.43	15.57	466.66	1		170.32	58.71	1760.20	2
	184.45	54.21	1625.31	2	$CO^{18}O$	646.856	15.459	463.461	1
$OO^{18}O$	253.64	39.43	1181.99		$^{13}CO^{18}O$	646.864	15.459	463.455	
	248.63	40.22	1205.80		CH_3OH	608.99	16.42	492.28	1
$O^{18}OO$	262.00	38.17	1144.25			556.65	17.96	538.57	
	256.38	39.01	1169.34		PH_3	561.61	17.81	533.81	1
$OO^{17}O$	251.29	39.79	1192.99			224.93	44.46	1332.85	2
	246.25	40.61	1217.46			187.56	53.32	1598.37	
$O^{17}OO$	264.24	37.85	1134.57			160.89	52.16	1863.36	
	253.02	39.52	1184.84			140.90	70.97	2127.69	

Table 9 Example ice and mineral transitions available with SAFARI-Lite.

Compound		Vibrational mode	Spectral range		SAFARI-Lite bands
			λ (μm)	ν (cm^{-1})	
Ices	H_2O[4]	Translational lattice: transverse optical, longitudinal optical, and longitudinal acoustic branches.	111 to 34	90 to 294	LW–SW
	CO[5]	Translational and librational lattice	222 to 100	45 to 100	VLW–LW
	αN_2[5]	Translational lattice	222 to 131	40 to 76	VLW–LW
	O_2[6]	Monoclinic base-centered Lattice (α-phase); Rhombohedral Lattice (β-phase)	200 to 74	50 to 135	VLW–MW
	HCN[7]	Librational lattice	70 to 40	143 to 250	MW–SW
	CO_2[5]	Translational lattice	167 to 74	60 to 135	VLW–MW
	CH_3OH[8]	Librational lattice	100 to 34	100 to 294	LW–SW
Minerals	Hibonite[9]	Spinel type lattice	120 to 34	83 to 294	LW–SW
	Talc[10,11]	Mg translational lattice	100 to 34	100 to 294	LW–SW
	Picrolite[10,11]	Mg translational lattice	105 to 37	95 to 270	LW–SW
	Montmorillonite[10,11]	Mg,Ca translational lattice	110 to 50	91 to 200	LW–SW
	Chamosite[10]	Lattice	160 to 65	63 to 154	VLW–MW
	Silica Polymorphs[12]	Lattice	80 to 34	125 to 294	MW–SW
	Fosterite[13]	Rhombic lattice	70 to 36	143 to 278	MW–SW
	Enstatite[13]	Rhombic/monoclinic lattice	80 to 34	125 to 294	MW–SW
	Calcite[14]	Transverse optical lattice	120 to 34	18 to 294	LW–SW
	Calcium–aluminum-rich inclusions[15]	Lattice	70 to 34	143 to 294	MW–SW

Science Theme 4: *Measure the abundances of CHNOPS-containing molecules and halides in the atmospheres of Venus and comets.* This theme would likely be part of the GO observing agenda, which is expanded on in Table 5 (see Sec. 2.5 for more details).

The unrivaled capabilities of SALTUS will enable solar system science to achieve significant advancement at submillimeter and far-IR wavelengths for comets, planetary atmospheres, the ocean worlds Enceladus, Europa, Titan, and possibly Ganymede, Callisto, and Triton, and other small bodies within our solar system, which will make significant progress toward resolving the fundamental questions of Where does Earth's water come from? and How did we get here? The following sections expand on the significance of each science theme and detail the extensive amount of solar system science achievable with SALTUS for both the GO and GTO observing programs. In particular, Sec. 2 gives science details for our GTO program (and some potential GO science) covering our four Solar System science themes. Section 2.2 concentrates on investigations of cometary HDO (Sec. 2.2.1), Enceladus' water torus (Sec. 2.2.2), the Galilean moons' water atmospheres (Sec. 2.2.3), and water elsewhere in the solar system (Sec. 2.2.4). Section 2.3 aims to determine the HD abundance in the Giant Planets, while Sec. 2.4 concentrates on icy particulates and minerals in the solar system. Section 2.5 highlights CHNOPS compounds and halides in the atmospheres of Venus and comets.

2.1 Threshold Versus Baseline Solar System Science

Year 1 of the SALTUS 5-year mission is dedicated to threshold science, where SALTUS will observe ~80 solar system objects, with 6 to 10 being a combination of Jupiter family comets (JFCs) and long-period or non-returning Oort cloud comets (OCCs). The threshold science will typically enable the initial detection and/or discovery of astrochemically relevant compounds for a significant number of targets, ranging from Venus in the inner solar system to KBOs in the cold outer solar system. The baseline science will then spectrally, spatially, and temporally expand on these pioneering measurements. The solar system scientific value of the threshold science is summarized in Tables 2–5, which also compare the measurement impact between the threshold and baseline sciences as they pertain to the four solar system science themes. This is given for all four themes and the GTO and GO observing agendas.

The GTO and GO science themes were constructed by the SALTUS Solar System Science team based on the needs of the science community as presented in the Decadal Survey and from NASA's goals/themes. Solar system GO science was constructed by the SALTUS Solar System Science team to demonstrate the full science capabilities of SALTUS beyond the GTO observational agenda. As such, these themes are by no means exhaustive, and we fully expect they will be modified during the GO program; hence, they should be taken as model science themes.

2.2 Science Theme 1: Following the Water Trail in Comets, Planets, Ocean Worlds, and Elsewhere in the Solar System

Among the strongest capabilities enabled by SALTUS are the HiRX instrument's high spectral resolving power ($R > 10^5$) and high detector sensitivity, which collectively enable measurements of numerous transitions of HDO, $H_2{}^{16}O$, $H_2{}^{18}O$, and $H_2{}^{17}O$. Science theme 1 will *trace the origin and history of water delivered to the solar system by observing the isotopologues in comets, ocean worlds, planetary atmospheres, and other known water reservoirs*. The measurements (see Table 2) include further observations of HDO in an additional 24 to 30 comets; water detection in the spatially extended Enceladus torus; water measurements in the tenuous atmospheres of Europa, Ganymede, and Callisto; and water in planetary atmospheres.

2.2.1 *Cometary HDO abundance*

Being among the most primitive known solar system bodies, comets are ideal cosmic laboratories for constraining the origin and thermal evolution of water in the solar nebula. D/H in water may depend on the distance of formation from the proto-sun and on when material incorporated into comets was last subjected to the gas-phase D/H exchange driven by vertical mixing between the disk midplane and photosphere. Reports of cometary HDO to date suggest an intrinsic dispersion spanning ~1 to 3 times that of Earth's oceans in cometary HDO/H_2O ratios (Fig. 3); however, these ratios have been reported for less than 20 comets, with several measurements representing upper limits. Furthermore, except for *in situ* measurements of two comets—one OCC[39] and one JFC[40]—HDO has not been measured simultaneously with H_2O. Therefore, the majority of HDO measurements are susceptible to systematic biases and uncertainties inherent to the diverse measurement techniques used and to potential time-varying water production for individual comets. SALTUS will address this severe shortfall, overcoming these innate uncertainties by simultaneously (or contemporaneously) observing HDO and H_2O in 30 to 40 comets during its 5-year lifetime using a single platform and employing a consistent measurement approach.

High accuracy in cometary D/H requires near-simultaneous measurements of H_2O lines with multiple HDO lines, which until now has been nearly impossible.[20] With its high spectral resolution, large collecting area, high sensitivity, and wide spectral range (allowing coverage of a large number of HDO and H_2O transitions), SALTUS HiRX 1 and 2 will provide a coherent and internally consistent set of HDO and H_2O observations that will allow—for the first time—an accurate determination of the HDO/H_2O ratios from both Oort cloud and (scattered) Kuiper belt reservoirs, representing the principal sources of OCCs and JFCs, respectively. In a single observing session, SALTUS HiRX observations will measure at least five HDO transitions between 112 and 645 μm in <12 h, which will significantly increase the sample size of reliably and contemporaneously measured HDO/H_2O ratios by an order of magnitude over the 5-year baseline mission. Moreover, few simultaneous measurements of HDO with other water isotopes exist, but

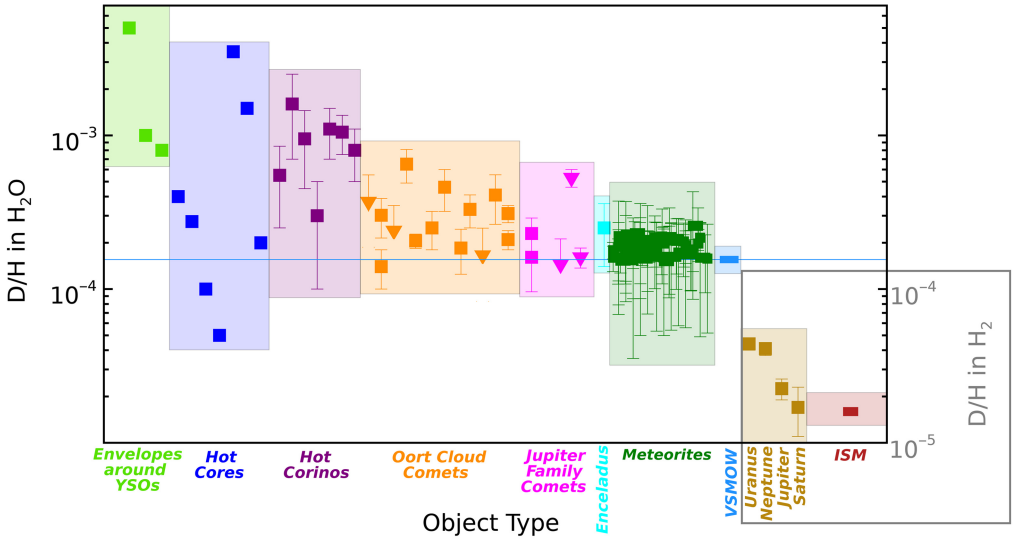

Fig. 3 D/H ratios in H_2O (left ordinate) and D/H ratios in H_2 (right ordinate; objects contained within the gray rectangular area) for numerous types of interstellar and solar system objects. The values for D/H in H_2O are given for three types of star-forming regions (collapsing envelopes and hot corinos, which are associated with low mass young stellar objects, and hot cores, which are associated with massive protostars), Oort cloud and Jupiter family comets, Enceladus' plumes, carbonaceous meteorites, and Earth's oceans (indicated by Vienna Standard Mean Ocean Water). D/H in H_2O reflects the minor reservoir of deuterium, which is highly fractionated as evidenced by the large spread in these values. Note that the D/H in water values represent the "cometary" notation; this value is half of the HDO/H_2O value. Likewise, the values for D/H in H_2, which are also indicated by the objects contained within the grey rectangle, are shown for the giant planet atmospheres and the interstellar medium and represent the major reservoir of elemental deuterium. The values provided for D/H in H_2 are also half the amount of the HD/H_2 abundance ratios. This figure reinforces that the interstellar and solar system measurements of numerous objects reveal considerable intrinsic dispersion that falls outside of the uncertainties corresponding to each individual measurement, reinforcing the need for high-accuracy measurements in D/H, which SALTUS is optimized to do. This figure is patterned after Ref. 16 that was originally adapted from Refs. 17–19, with inputs from Refs. 20–38.

the proposed HiRX observations will simultaneously measure lines of $H_2{}^{16}O$, $H_2{}^{18}O$, and $H_2{}^{17}O$ with HDO, necessary to retrieve precise isotopic ratios. Specifically, measuring $H_2{}^{18}O$ and $H_2{}^{17}O$ for more productive comets will address potential opacity issues in $H_2{}^{16}O$ lines, thereby enabling accurate water production rates and D/H ratios. Figure 4 shows a simulated comet spectrum for SALTUS HiRX 1 and 2, demonstrating the wealth of molecular information available with HiRX in a single SALTUS observing session. In the radiative transfer model, the following values were adopted: water production rate = 1×10^{28} molecules/s, heliocentric distance = 1.2 au, geocentric distance = 1.0 au, gas temperature = 50 K, outflow velocity = 0.70 km/s, and molecular abundances and terrestrial isotopic ratios (2% CH_3OH, 0.6% H_2S, 0.5% NH_3) from Refs. 41 and 42.

Simultaneous observations of HDO and $H_2{}^{18}O$ in HiRX 1 and HiRX 2 are required because the resulting measurements will sample spatially different regions of the cometary coma and, hence, different temperatures. The four lowest levels of HDO in HiRX 1 and HiRX 2, combined with numerous CH_3OH lines, will be used to retrieve rotational temperatures (see Tables 7 and 8). For $H_2{}^{16}O$, HiRX 2 will be solely used to measure numerous lines because the few transitions available in HiRX 1 are either too strong (saturated) or too weak (too long of an integration). The SALTUS unparalleled capability to operate HiRX 1 and HiRX 2 in tandem allows for long integrations of HDO and $H_2{}^{18}O$ in HiRX 1 while simultaneously conducting short integrations on $H_2{}^{16}O$ and the stronger transitions of HDO, $H_2{}^{18}O$, and $H_2{}^{17}O$ in HiRX 2 and then while still integrating in HiRX 1, independently frequency tuning HiRX 2 across its full spectral range to acquire additional transitions of these species, all in a single comet observing session.

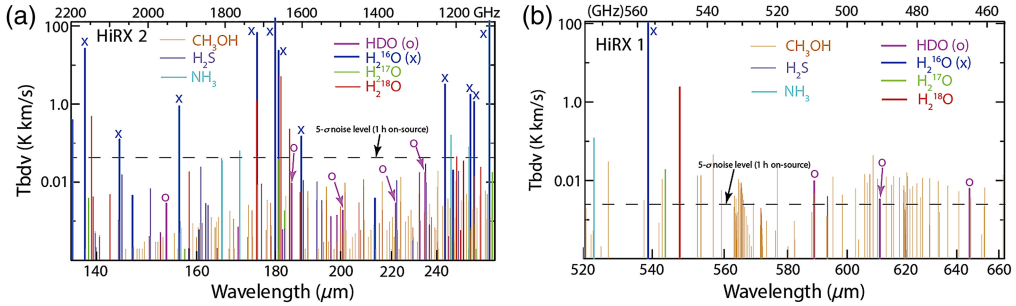

Fig. 4 Simulated HiRX band 2 (a) and band 1 (b) brightness temperature spectra for a typical comet with a gas production rate of 10^{28} molecules s^{-1} and at a distance of 1 AU from SALTUS. This figure reveals a plethora of emission lines falling within these two HiRX bands. This demonstrates how SALTUS will measure HDO, $H_2{}^{16}O$, $H_2{}^{18}O$, and $H_2{}^{17}O$, together with other key molecules, simultaneously or near-simultaneously, due to frequency tuning in 750 MHz or 4 GHz (band 1) and 3.5 GHz (band 2) instantaneous bandwidths (Sec. 1), to build up composite spectra across the full spectral ranges of HiRX bands 1 and 2. Prominent lines of $H_2{}^{16}O$ (marked by x) and HDO (marked by o) are labeled, and all lines are color-coded by species or water isotope, with the 5σ noise levels for 1 h of on-source integration time superimposed (long dashed horizontal line running across each panel).

For more productive comets, measurements of $H_2{}^{18}O$ and $H_2{}^{17}O$ in HiRX 2 will address potential opacity issues in $H_2{}^{16}O$ lines, thereby enabling more precise water production rates. For rotational temperatures between 40 and 70 K, the most favorable HDO lines are those at 234.8, 184.5, and 153.7 in HiRX 2 and at 589 μm and (co-measured with CH_3OH) at 610.6 μm in HiRX 1.

2.2.2 *Enceladus' water torus*

Saturn's moon Enceladus is a prime target for investigating the habitability of an ocean world. The Cassini–Huygens mission discovered Enceladus' subsurface liquid water reservoir, which ejects water vapor at a mass flow rate of hundreds of kg/s, by way of four ~2-km-wide cracks residing poleward of ~70°S.[43–45] Enceladus' plume ejecta have a substantial impact on the Saturn system, in which the escaping water vapor and ice particles are responsible for (i) coating the surfaces of many moons and main ring particles with water ice,[46,47] (ii) generating Saturn's E-ring (Ref. 48 and references therein), and (iii) initially forming a narrow torus around Saturn that spreads to a spatially diffuse torus, which Herschel HIFI discovered to vertically extend tens of thousands of kilometers;[49] this is the prime source of Saturn's upper atmospheric water.[50]

The large spatial extent of Enceladus' torus (Fig. 5) offers SALTUS a unique opportunity to map the spatially varying $H_2{}^{16}O$ abundances and HDO and $H_2{}^{18}O$ isotopic abundance ratios, along with important non-water molecules, all critically needed to probe conditions in the interior of an ocean world. Recent JWST Near-Infrared Spectrograph (NIRSpec) measurements demonstrated its sensitivity in the near-IR to solar-pumped fluorescence emissions of $H_2{}^{16}O$ vapor residing from within and beyond Enceladus' plumes.[51] Several non-water species (CO_2, CO, CH_4, C_2H_6, CH_3OH) as well as the water isotopologues HDO, $H_2{}^{18}O$, and $H_2{}^{17}O$ went undetected by JWST. SALTUS HiRX is optimized to detect the low energy transitions of water and its isotopologues ($H_2{}^{16}O$, $H_2{}^{17}O$, $H_2{}^{18}O$, HDO), along with key non-water species such as CO, NH_3, HCN, CH_3OH, and H_2S at high spectral resolving power ($R > 10^5$). A considerable advantage of SALTUS over JWST is that HiRX 2 will be used to detect water emission signatures over the full spatially extended torus, rather than being restricted to within 2″ of Enceladus. SALTUS HiRX 1 and 2 measurements will also expand on the Herschel legacy by measuring the same $H_2{}^{16}O$ transitions at 538.3 and 179.5 μm but with higher spatial resolution (3.2″ at 179.5 μm compared with Herschel's 12.9″). Since Enceladus (0.07″) was unresolved by Herschel, SALTUS can take advantage of its large aperture and resulting factor of 16 increased sensitivity to measure a wealth of additional water lines and accurately establish the torus gas

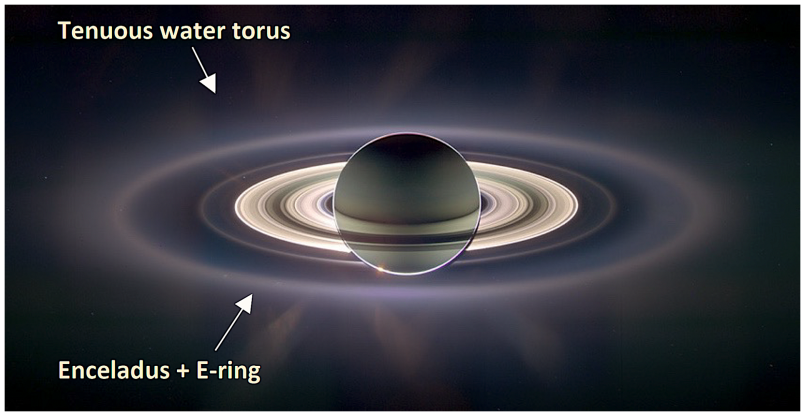

Fig. 5 SALTUS will measure the spatial variation of Saturn's tenuous water torus encompassing the planet, resulting from the water emanating from Enceladus' plumes. Although the water phase in Saturn's equatorial plane is predominantly ice, as indicated in this figure, gaseous water from Enceladus' plumes that reaches escape velocity is responsible for the tenuous water torus that vertically extends tens of thousands of kilometers above Saturn's ring plane.[17] SALTUS HiRX bands 1 and 2 will observe numerous low-excitation energy water lines emitting from both the Saturn and Jupiter systems, necessary to resolve the external sources of water delivered to these giant planets. Saturn image credit: NASA/JPL/Space Science Institute.

temperature. These cutting-edge measurements will help inform on Questions E-Q3a,b in Astro2020:[1] How are potentially habitable environments formed? What processes influence the habitability of environments?

2.2.3 *Galilean moons' water atmospheres*

SALTUS will conduct repeated observations of the strongest water lines (e.g., 538.3 and 179.5 μm) at Ganymede, Callisto, and Europa as functions of their orbital positions (e.g., illumination, leading versus trailing hemispheres) to constrain the processes responsible for maintaining these ocean world atmospheres. Models have predicted the quantity of water vapor and its spatial distribution due to sputtering, radiolysis, and sublimation (e.g., for Europa,[52,53] Ganymede,[54] and Callisto[55]). For example, for Europa, these models predict a total mass of the water atmosphere to be on the order of 20 to 100 metric tons, significantly lower than the values predicted for Ganymede and Callisto and too low to be detected from ground-based observations. Transient events (e.g., plume activity) have been reported[56,57] that are consistent with ~2000 tons of total water, yielding a detection limit of ~500 tons. SALTUS' HiRX 2 observations are three orders of magnitude more sensitive, i.e., for an integration time of 1 h, detection limits of ~1 ton are anticipated with HiRX 2. The high sensitivity of SALTUS enables the detection of the "quiescent" water atmospheres of Europa, Ganymede, and Callisto, without the need for transient events. This will help constrain the respective roles played by these processes and is complementary to ESA's JUICE mission science and NASA's Europa Clipper mission science,[58–60] both spacecraft arriving at Jupiter in the 2030–2031 time frame, which shortly precedes the commencement of the SALTUS phase-E mission.

2.2.4 *Water elsewhere in the solar system*

With HiRX 1 and 2, SALTUS will measure H_2O abundances in the stratospheres of the gas giants to determine whether planetary rings, icy moons, interplanetary dust particles, or comet impacts are responsible for delivering water to these planets. Saturn's largest moon Titan, another Ocean World, has a complex atmosphere comprising oxygen compounds that were likely delivered from the Enceladus-generated water torus surrounding Saturn.[61–63] SALTUS will measure the vertical and horizontal distributions of H_2O in Jupiter's and Saturn's stratospheres with unprecedented spatial resolution compared with previous observations[50,64–66] to determine the relative magnitude of the various external sources and their temporal variability. Although Herschel fell short in

resolving Uranus by more than a factor of 10,[67] SALTUS will spatially resolve both ice giants for the first time, which has proven to be critical to determine the main external source of H_2O delivered to Jupiter and Saturn.[50,65] Moreover, water vapor emission has been observed from the dwarf planet, Ceres; although, the source of water and its spatial distribution remains unknown. SALTUS' high sensitivity will permit us to establish whether ice sublimation or cryo-volcanism from localized regions is the source of Ceres' observed water. In addition, SALTUS will measure the abundance of H_2O and HDO in Venus' atmosphere to better understand its evolution over time.

2.3 Science Theme 2: HD Abundance in the Giant Planets' Atmospheres

HD represents the bulk reservoir for deuterium in the giant planets' atmospheres. Unlike terrestrial planets, giant planets have not experienced significant atmospheric escape; thus, the present-day deuterium abundances in their atmospheres are expected to represent their primordial value. Jupiter's immense H_2-dominated atmosphere far exceeds the mass of its presumed core; thus, Jupiter's D/H ratio is presumed to reflect the protosolar value. The measured D/H in hydrogen is smaller on Saturn than on Jupiter,[69] which is unexpected, and the mechanism for depleting HD is not well understood. In the ice giant atmospheres, D/H is observed to be roughly twice the value as in the gas giants, therefore enhancing the contribution of the ice-producing D in HD's final abundance post equilibrium.[70] Their factor of 4 to 10 lower D/H compared with comets, coupled to their high internal carbon and oxygen abundances,[71,72] however, remains unexplained.

Science theme 2 will measure the D/H ratio in HD in the giant planets to constrain their formation, which will confirm or refute the expectation that HD is well mixed. This includes spatial maps of HD on Jupiter and Saturn, along with methane, to determine whether D/H varies with latitude. Accurate D/H measurements are needed to constrain giant planet origin models, and HD can only be observed from air- and space-borne platforms. Herschel's PACS,[70,73] the ISO LWS,[69] and Cassini CIRS[74] measured HD in the giant planets, but all the measurements lacked sufficiently high spectral resolution to separate stratospheric emission from tropospheric absorption (see Fig. 6), thus limiting the accuracy in deriving HD/H_2 abundance ratios. This problem will be alleviated with measurements obtained from the SALTUS HiRX instrument, which is designed to target the HD 1-0 transition at 112.1 μm (HiRX 3) and the HD 2-1 transition at 56.2 μm (HiRX 4b) with a resolving power of 1×10^6. As demonstrated in Fig. 6, these high spectral resolution measurements will spectrally resolve the HD emission line cores, enabling the derivation of stratospheric D/H for the giant planets. While HD is expected to be well mixed, SALTUS will quantify this by independently measuring D/H in the upper tropospheres (from broad absorption features) and stratospheres (from narrow emission line cores) of the giant planets, thus separating both contributions, and with an improved spatial resolution of 2.0″ at 112.1 μm over 9.4″ for Herschel PACS and 47.0″ for ISO LWS. For reference, the average angular diameters from Earth are 40″ (Jupiter), 17″ (Saturn), 3.7″ (Uranus), and 2.3″ (Neptune).

2.4 Science Theme 3: Icy Particulates in the Solar System

The far-IR is a robust spectral region that comprises low-energy intermolecular and lattice vibrational modes of many astrophysically relevant ices, providing unique views into the ice composition, structure, porosity, and thermal history. The uniqueness of the lattice modes enables us to easily distinguish between the amorphous and crystalline ice phases, opening a window to phase transition temperatures, which ultimately constrains the thermal evolution of the ice. For example, H_2O ice translational mode spectra depend on the crystal structure and change from two well-defined, sharp features at ~43 and ~62 μm for crystalline ice to a broad band at ~45 μm for amorphous ice[4] (Fig. 7). For crystalline H_2O ice, the peak position is a good thermometer as the band narrows with a distinct peak near 43 μm but also shifts systematically by 2 μm as the crystalline water ice cools from ~145 to 20 K (see black and maroon color-coded curves in Fig. 7). Lattice modes are also sensitive to the ice microscopic structure, in which porosity in many ways controls the surface chemistry and photolysis of interstellar ices. Moreover, ice lattice modes are the best viable way to determine the presence of homo-nuclear molecules such as O_2 and N_2, whose fundamental modes are IR inactive. Although ice phase transitions are observable in the near- and mid-IR, they are appreciably more difficult to discern because the band shapes are less distinguishable than those in the far-IR.

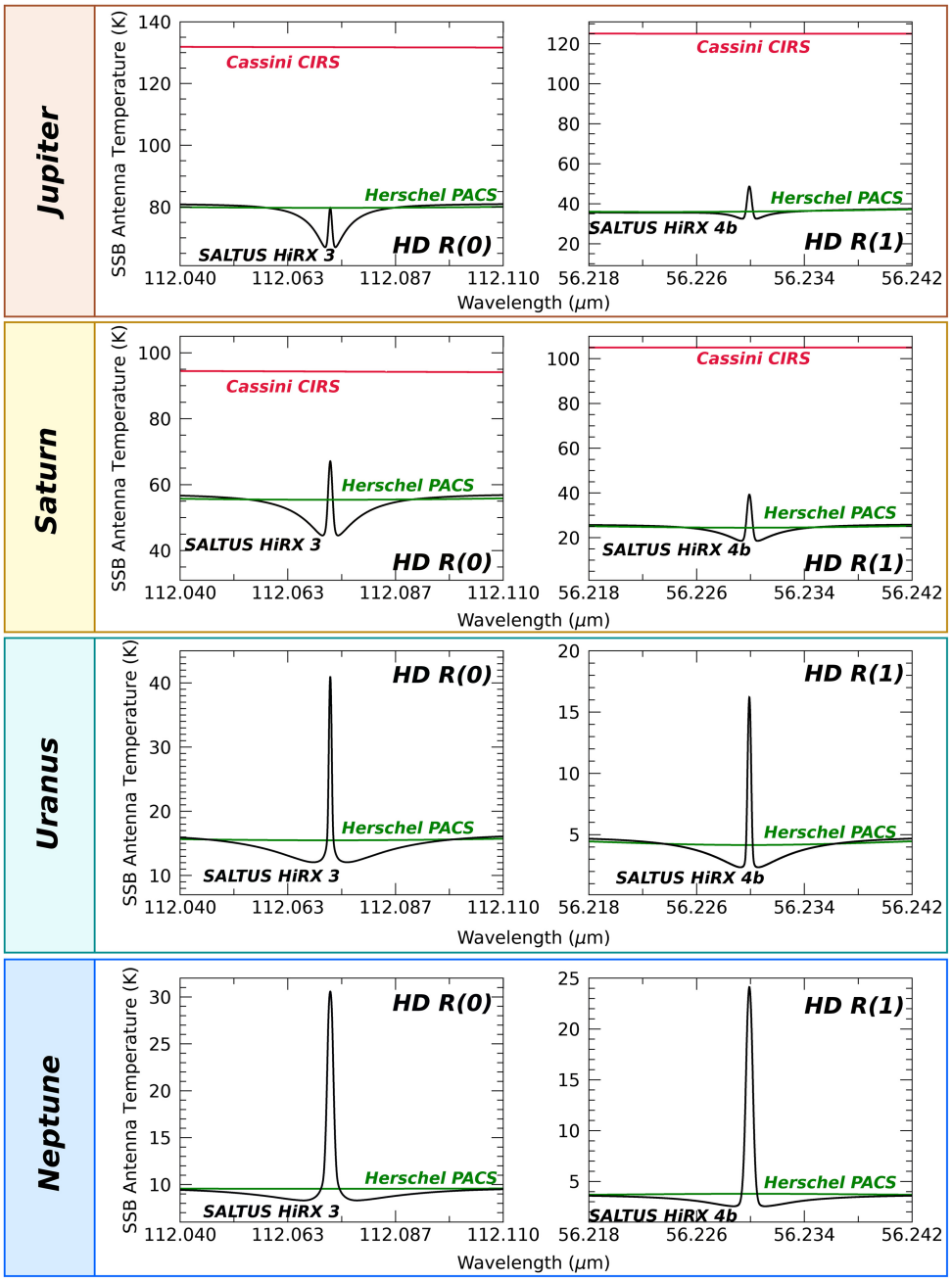

Fig. 6 Calculated HiRX spectra of the $R(0)$ line of HD at 112 μm (left column) and the $R(1)$ line of HD at 56 μm (right column) for each of the giant planets (rows). The single side band antenna temperature is shown as a function of wavelength calculated at a resolving power of 1×10^5. Although SALTUS/HiRX bands 3 and 4b have higher spectral resolving power ($\sim 1 \times 10^6$, see Table 1), the fast rotation ($\sim$30 km/s) of the giant planets broadens these HD lines. The HD mole fractions used in this simulation were derived from Herschel/PACS,[70,73] ISO/LWS,[69] and Cassini/CIRS observations[74] of these planets. A prominent HD emission core sounds the stratosphere of each planet, whereas the broad absorption feature originates from the troposphere. These line shapes will yield the most accurate measurement of the D/H ratio for all of the giant planets, as well as any vertical gradient in this value between the troposphere and stratosphere. Superimposed are the measurements from Herschel PACS (green) for the giant planets and from Cassini CIRS (red) for the gas giants. As depicted, both Cassini CIRS and Herschel PACS lacked sufficiently high spectral resolution to separate the stratospheric narrow emission line cores from the tropospheric broad absorption features, which SALTUS HiRX is optimized to do. The use of two HD transitions with SALTUS permits solving for both temperature and abundance. The temperature profile of each planet will also be constrained by nearly simultaneous measurements by SALTUS of CO, CH_4, and the continuum produced by collision-induced absorption of $H_2 - H_2$ and $H_2 - He$.

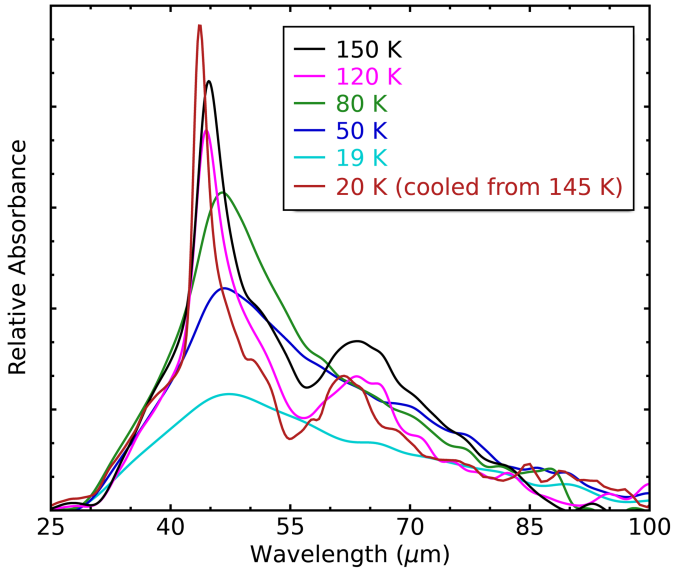

Fig. 7 Thin ice film transmittance spectra of the far-IR phonon modes of water ice at vapor deposition temperatures of 19 (aqua), 50 (blue), 80 (green), 120 (pink), 150 (black), and 20 K (maroon; gas was deposited at 145 K into the crystalline phase then cooled to 20 K).[75] As H_2O ice transitions from disordered amorphous (19 K), to more ordered amorphous (80 K), and ultimately to the crystalline phase (150 K), the far-IR spectral features greatly sharpen, revealing two distinctive crystalline phonon vibrational modes near 43 and 62 μm. This spectral behavior with temperature enables discrimination from the amorphous-to-crystalline state, demonstrating its sensitivity to thermal history and ice structure. The maroon curve demonstrates how the peak position of crystalline water ice acts as an excellent thermometer because the peak near 43 μm shifts systematically by 2 μm as the crystalline ice cools from 145 to 20 K. SALTUS SAFARI-Lite measurements will significantly extend our understanding of near-IR detected ices through their far-IR characterization.

The SALTUS SAFARI-Lite instrument will make history by exploiting the far-IR spectral regime to retrieve spectral signatures of a profound number of chemically distinct ices, most notably H_2O, N_2, O_2, CO_2, CO, CH_3OH, CH_4, H_2S, and HCN (see Fig. 1 and Table 9) in cometary and planetary atmospheres and on icy moon and outer solar system small body surfaces. As a result of its simultaneous spectral coverage of the full 34 to 230 μm range and its high sensitivity, SAFARI-Lite is uniquely suited to study the diagnostic lattice modes of ices in solar system objects, providing temperature, mass, and structure of the emitting ices. The purpose of these measurements is to quantify the amount of ice, its emission temperature, and its structure (amorphous versus crystalline) and relate these characteristics to the gas mass and temperature in the environment being studied, allowing a direct comparison between the solid and gaseous reservoirs.

A systematic study of far-IR ices from previous far-IR space missions, such as Spitzer, Herschel, and ISO, was not possible due to the lack of wavelength coverage or sensitivity. Studies with ISO were limited by sensitivity because the 30- to 100-μm wavelength range was covered by two spectrometers with very different footprints. On the other hand, the Herschel/PACS spectrometer was designed for studies of gaseous emission lines and had a very small wavelength coverage in any single setting. Detection of spectrally broad ice features required the careful stitching of many individual wavelength settings, a procedure fraught with issues as small pointing drifts caused a spurious spectral structure that was difficult to correct.

The sensitivity, spectral resolution, and broad wavelength coverage of SAFARI-Lite also make it an ideal instrument to measure the spectral signatures of mineral grains (see Table 9 and Fig. 8) in cometary comae, which constrain the comet's physical characteristics. IR spectroscopic studies of silicate emission have proven to be a valuable tracer of grain processing as the detailed spectral signature of the emission bands is very sensitive to structure, composition, and temperature of the emitting grain (Fig. 8). SAFARI-Lite will observe solid-state resonances from dust particles in the far-IR with unprecedented sensitivity, covering simultaneously the 34- to 230-μm spectral region that is key to identify minerals through their characteristic vibrational

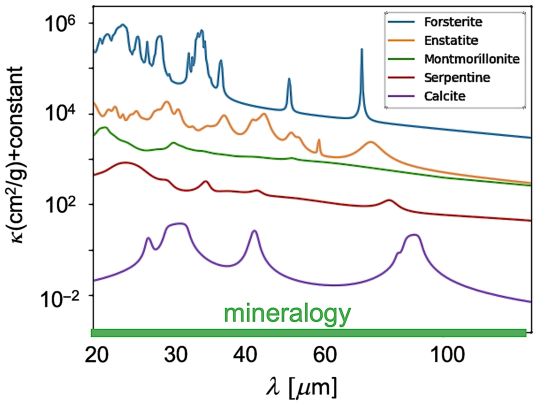

Fig. 8 Example far-IR spectral signatures of the minerals forsterite (Mg_2SiO_4), enstatite ($MgSiO_3$), calcite ($CaCO_3$), and the hydrosilicates montmorillonite ((Ca0.5,Na)0.7(Al,Mg,Fe)4(Si,Al)8O20(OH)4nH2O) and serpentine ((Mg,Fe)6Si4O10(OH)8), showing SAFARI-Lite's potential to detect and identify these minerals. This figure was reproduced from Ref. 76. 2021 © Cambridge University Press, reproduced with permission.

resonances (Fig. 8). Science theme 3 will therefore investigate the role of both ices (Sec. 2.4.2) and minerals (Sec. 2.4.5) contained within comets, ices in planetary atmospheres, ices near Enceladus' plumes (Sec. 2.4.1), and ices on the surfaces of icy moons (Sec. 2.4.3), Jupiter trojans, centaurs, and KBOs (Sec. 2.4.4). These measurements include far-IR observations of numerous ices, along with mineral features (Table 4), in 24 to 30 cometary comae, in the atmospheres of the giant planets and Titan, and near Enceladus' plumes.

2.4.1 *H_2O ice in Enceladus' plumes*

The water ice abundance in Enceladus' tenuous and cold plumes is extremely low, with a derived plume water ice number density of ~0.004 particles/cm^3 at a 50-km altitude, based on Cassini visual and infrared mapping spectrometer (VIMS) measurements.[77] VIMS operated in the near-IR between 1 and 5 μm, sensitive to the light scattered by the plume water ice particles. The strong and broad O–H stretching mode of water ice fell within the VIMS bandpass, resulting from the nearly concurrent ν_1 and ν_3 fundamental modes. The water ice fundamental modes have complex spectroscopic signatures that are modulated by both temperature and ice phase, requiring rigorous radiative transfer modeling (coupled with Mie scattering and ice experimental efforts) for interpretation. There is, however, a weak spectral feature at 1.65 μm that is typically associated with crystalline water ice because, when amorphous, the feature becomes suppressed.[78,79] The VIMS spectral resolution was coarse, so 1.65 μm was difficult to detect, but recently, it was confirmed with JWST NIRSpec measurements of Enceladus' extended plume.[51] The SALTUS SAFARI-Lite measurements are complementary to both Cassini and JWST and will help broaden our current understanding of Enceladus' water inventory by enabling spectral mapping of the E-ring ice composition around Enceladus' orbital position at a spatial resolution of 0.8″ at 45 μm. These measurements will enable a more thorough characterization of water ice in and around Enceladus' plumes; this includes the plume-ejected ices that remain in Saturn's equatorial plane to form the E-ring. One advantage SALTUS has over JWST is that SAFARI-Lite is optimized to detect the far-IR (i.e., thermal-IR) signatures of water ice, arising from distinctive lattice phonon vibrational modes, allowing for discrimination between the crystalline and amorphous phase states, in/near the plume and in the E-ring. These phonon modes have significantly more pronounced differences in their spectral dependencies at a given temperature (illustrated in Fig. 7), compared with the fundamental modes in the near-IR, resulting in far less interpretational errors in identifying the specific ice phase.

2.4.2 *Gas trapping in amorphous ice*

One of the most unanticipated results from the Rosetta mission was the discovery of an O_2 reservoir (1% to 10% O_2/H_2O abundance ratio) in comet 67P/Churyumov–Gerasimenko.[80]

As H_2O, CO_2, and CO comprised 95% of the total volatile inventory abundance, the high abundance of O_2 is indicative of it having a primordial origin, most likely incorporated into 67P's nucleus during the comet's formation. The O_2 inventory may have emanated from the radiolysis of amorphous water ice, where O_2 became trapped and preserved until the nucleus underwent some warming.[80,81] As water ice transitions from a disordered amorphous structure to a more ordered amorphous structure and, ultimately, to an ordered crystalline structure, the bulk ice structure becomes less porous. The more porous the ice, the more sites are available to trap volatiles such as O_2. As the comet's nucleus experiences warming, the amorphous ice structure will become less disordered, thus reducing the number of available sites for trapped volatiles—a sink process for O_2. The Rosetta mission's detection of highly abundant O_2 implies that comet 67P has not experienced high-enough temperatures; otherwise, O_2 vapor would have escaped over time as the amorphous ice would inevitably transition to [or close to] the crystalline phase with warm-enough temperatures. The SAFARI-Lite measurements will be of vital importance given that the far-IR spectral signatures of water ice (and other species) are as unique as fingerprints and consequently are sensitive to thermal history and ice structure.

2.4.3 *Non-polar ices*

As a non-polar molecule, the fundamental modes of N_2 in the IR, along with its corresponding overtone and combination bands, should be inactive. This is not the case, however, at least regarding decades worth of Triton observations, in which weak absorption bands at 2.15 μm have been observed on its surface, as was observed by the New Horizons LEISA spectrometer during the Pluto flyby,[82] and attributed to the first overtone band of the 4.26-μm fundamental mode of βN_2 ice.[83] The presence of the weak 2.15-μm feature indicates that the 4.26-μm fundamental stretching mode of N_2 has been perturbed in the ice phase, most likely via interactions with adjacent compounds.[84–86] Ground-based IR spectroscopy of Triton's surface only exists between 1 and 2.5 μm due to low S/N ratios and terrestrial atmospheric opacity issues because Earth's atmosphere is opaque at 4.3 μm due to CO_2 gas. As a result, Triton surface observations could not resolve the N_2 ice fundamental feature at 4.26 μm, which is needed to confirm or refute the identification of pure N_2 ice from its overtone band at shorter wavelengths because fundamental modes are inherently stronger than their overtone bands. Recently, JWST spectroscopy, spanning 0.9 to 5.3 μm, revealed the 2.15-μm N_2 feature on two hemispheres of Triton.[87] Multiple absorption features of CO_2 ice were also observed, with the strongest CO_2 ice feature at 4.3 μm. This strong absorption feature results from a mixture of N_2 ice and CO_2 ice, which would be difficult to use to retrieve ice abundance. To disentangle the individual spectral signatures of each ice within this mixed ice is much more difficult at the shorter, near-IR JWST wavelengths. However, with SAFARI-Lite far-IR spectroscopy of the ice low-energy phonon vibrational modes, in combination with laboratory thin ice film spectroscopy measurements, the absolute contribution from each ice species within the mixture can easily be extracted.

2.4.4 *Ices on small bodies*

Using its full spectral range, the SAFARI-Lite instrument enables spectral surveys of the chemically distinct lattice modes of numerous ices on the surfaces of Jupiter trojans, centaurs, and KBOs (i.e., trans-Neptunian objects and Pluto). Active centaurs—small bodies transitioning from Kuiper disk orbits into Jupiter family comet orbits—are of particular interest to the science community given their observed time-variable CO-dominated comae.[88,89] There is a real mystery as to what drives the time-variable CO in these active centaurs. A plausible explanation may be a similar gas-trapping mechanism as with O_2 in comets, which SAFARI-Lite measurements will significantly help to unravel.

The era of JWST has enabled studies of KBOs and other outer solar system objects in reflected sunlight. Building on these measurements but in the thermal-IR, SAFARI-Lite, as part of the SALTUS GO program, is uniquely capable of extending our knowledge and characterizing these cold outer solar system objects at the long wavelengths in the far-IR.

2.4.5 *Astromineralogy*

The first step in the formation of planetesimals and cometesimals—the building blocks of planets—is the agglomeration of small dust grains inherited from the interstellar medium. Interstellar grains are modified by nebular processes, which are recorded in the detailed spectroscopic characteristics of aggregates making up these bodies and can be "read" by IR observations. Mid-IR spectroscopy has revealed that interstellar silicates are predominantly amorphous in nature,[90] whereas silicates in the planet-forming disks associated with Herbig Ae/Be and T Tauri stars have a significant crystalline component.[91,92] In the solar system, asteroidal and cometary grains also have a high crystalline fraction,[93–96] and the spectral signatures of mineral grains in cometary comae constrain the comet's physical characteristics. For example, ISO SWS measurements revealed the abundant presence of forsterite, the Mg-rich end member of olivine (Mg_2SiO_4) that dominates the IR emission spectrum of comet Hale-Bopp.[93] The peak position of the 69-μm mode is extremely sensitive to both the iron content and the temperature of the emitting dust. Another example involves phyllosilicates (OH-bearing magnesium and iron silicates), important constituents of primitive meteorites, and thus are likely to be present on the surface of outer solar system objects beyond the center of the main asteroid belt at 2.5 AU. Lattice modes of O–H in these minerals exhibit strong absorption features at 39 and 60 μm in talc and at 43 and 77 μm in picrolite.[10] SAFARI-Lite broadband spectra of small solar system objects will yield critically important information on the degree of hydration and, thus, the interaction between water and silicates over the history of these bodies.

2.5 Science Theme 4: CHNOPS Compounds and Halides in Comets and Venus

Sulfur compounds on Venus are of interest not only for understanding its sulfuric acid clouds but also as tracers of either ongoing volcanism[97] or episodic exchanges with the sulfur-rich lower atmosphere.[98] SALTUS HiRX 1 and 2 will measure SO_2, SO, OCS, and H_2S (see Table 8) to understand these processes better.[99,100] SALTUS will exploit the rich submillimeter and far-IR spectrum to search for new sulfur compounds, possibly revealing the identity of a chemically unknown sulfur source observed by Venus Express between 70 and 100 km.[101]

Venus observations from both ALMA and James Clerk Maxwell Telescope resulted in the controversial identification of PH_3 in its atmosphere, which was reported to be a potential biosignature by Ref. 102. The reported detection has been considerably disputed by several re-analyses of the submillimeter data[103–105] and by its absence in IR spectra at shorter wavelengths.[106,107] In view of phosphine's significance to both astrobiology and our understanding of Venus and exo-Venus' atmospheres, the combination of the SALTUS HiRX bands 1 and 2 enables measurements of five separate transitions of PH_3 (see Table 8). Thus, SALTUS, with its high spectral and spatial resolution, will be able to confirm or refute the existence of PH_3 in Venus' atmosphere above the cloud tops (see Ref. 16 for radiative transfer simulations depicting these five transitions).

The halides, HCl and HF, are the main halogen-bearing molecules in cometary comae. HF was only marginally detected with Herschel in one comet[108] and HCl recently in the infrared in comet C/2021 A1 (Leonard).[109] Herschel observations of HF and HCl and the IR detection of HCl point to abundances on the order of 0.02% relative to water at most. *In situ* observation in the coma of comet 67P confirmed similar abundances with a mean Cl/O of 0.012% and F/O of 0.009%, from mass spectrometry.[110] The chlorine abundance in comets looks depleted by a factor of 6 compared with the solar value, whereas fluorine in 67P is solar. The $H^{35}Cl(2-1)$, $H^{37}Cl(2-1)$, and HF(1-0) lines will be detected in several bright comets every year with SALTUS HiRX band 2, together with H_2O lines to assess the abundance of hydrogen halides and their variation from comet to comet.

Science theme 4 will therefore measure the abundances of CHNOPS-containing molecules and halides in the atmospheres of Venus and comets (see Table 5). These measurements include spectral surveys using the full spectral range of HiRX 1 and 2 of numerous transitions of O_2, O_3, CH_4, N_2O, NH_3, CO_2, OCS, SO_2, HF, HCl, and CO, in 30 to 40 comets, and will search for abundance variations as functions of latitude, longitude, altitude, and local time, targeting transitions of CO, O_2, O_3, H_2S, H_2SO_4, ClO, H_2O_2, SO, SO_2, OCS, NO, NO_2, and PH_3 in Venus' middle atmosphere.

3 Concluding Remarks

SALTUS will be a powerful far-IR space observatory that offers unique capabilities, which are unavailable from other space platforms. The combination of its sensitive heterodyne receiver system, HiRX (wide far-IR spectral regime rich in numerous molecular species and isotopologues at $R = 10^5$ to 10^7) and SAFARI-Lite (continuous spectral coverage from 34 to 230 μm at $R = 300$), all coupled to high spatial resolution, offers a robust tool for compositional studies of solar system gases, ices, and minerals. As mentioned in Sec. 2, the SALTUS Solar System Science team constructed science themes based on the needs of the science community as portrayed in the Decadal Survey and from NASA's goals/themes. The specific GTO goals serve to highlight SALTUS performances to illustrate the science capabilities possible for the GO program, with the GTO investigations comprising at most 25% of available observatory time; hence, the vast percentage of observing time will be formulated by the science community in the GO program. SALTUS is truly a community resource, and there are a significant number of high-impact measurements possible with the GO program beyond the model GO science themes. For details on the GO program, see the SALTUS observatory's overview paper by Chin et al., "Single Aperture Large Telescope for Universe Studies (SALTUS): Probe Mission and Science Overview" (this issue). For additional information on the type of solar system science made possible from a space observatory with an instrument nearly identical to HiRX (excepting Band 4b), see Ref. 16, which provided an expanded science discussion for the bulk of the HiRX-targeted science discussed in this present paper, and additional science content regarding Titan, Triton, Ceres, and the moon, along with radiative transfer simulations of Venus' middle atmosphere, Titan's stratosphere, and water vapor in the giant planet stratospheres.

Disclosures

The authors have no relevant financial interests in the paper and no other potential conflicts of interest to disclose.

Code and Data Availability

This paper reviews the science and observations for a future space observatory, so data sharing is not applicable at this time.

References

1. E. National Academies of Sciences and Medicine, *Pathways to Discovery in Astronomy and Astrophysics for the 2020s*, The National Academies Press, Washington, DC (2021).
2. C. Kouveliotou et al., "Enduring quests-daring visions (NASA astrophysics in the next three decades)," arXiv:1401.3741 (2014).
3. G. L. Villanueva et al., "Planetary spectrum generator: an accurate online radiative transfer suite for atmospheres, comets, small bodies and exoplanets," *Quantum Spectrosc. Radiat. Transf.* **217**, 86–104 (2018).
4. R. G. Smith et al., "Molecular ices as temperature indicators for interstellar dust: the 44- and 62-μm lattice features of H_2O ice," *Mon. Not. R. Astron. Soc.* **271**, 481–489 (1994).
5. A. Ron and O. Schnepp, "Lattice vibrations of the solids N_2, CO_2, and CO," *J. Chem. Phys.* **46**, 3991–3998 (1967).
6. I. Y. Fugol, I. M. Pritula, and L. V. Khashchina, "IR-active lattice absorption of the α- and β-phases of oxygen in the 45 to 150 cm-1 region," *Phys. Status Solidi B Basic Res.* **170**, 615–622 (1992).
7. C. M. Anderson et al., "The SPECTRAL ice chamber: application to Titan's stratospheric ice clouds," *Astrophys. J.* **865**, 62 (2018).
8. B. M. Giuliano et al., "Interstellar ice analogs: H_2O ice mixtures with CH_3OH and NH_3 in the far-IR region," *Astron. Astrophys.* **592**, A81 (2016).
9. H. Mutschke et al., "Towards the identification of circumstellar hibonite," *Astron. Astrophys.* **392**, 1047–1052 (2002).
10. H. Mutschke et al., "Far-infrared spectra of hydrous silicates at low temperatures. Providing laboratory data for Herschel and ALMA," *Astron. Astrophys.* **492**, 117–125 (2008).
11. A. M. Hofmeister and J. E. Bowey, "Quantitative infrared spectra of hydrosilicates and related minerals," *Mon. Not. R. Astron. Soc.* **367**, 577–591 (2006).
12. C. Koike et al., "Infrared spectra of silica polymorphs and the conditions of their formation," *Astrophys. J.* **778**, 60 (2013).

13. C. Jaeger et al., "Steps toward interstellar silicate mineralogy. IV. The crystalline revolution," *Astron. Astrophys.* **339**, 904–916 (1998).
14. T. Posch et al., "Carbonates in space: the challenge of low-temperature data," *Astrophys. J.* **668**, 993–1000 (2007).
15. T. Posch et al., "Infrared spectroscopy of calcium-aluminium-rich inclusions: analog material for protoplanetary dust?" *Astrophys. J.* **656**, 615–620 (2007).
16. C. M. Anderson et al., "Solar system science with the orbiting astronomical satellite investigating stellar systems (OASIS) observatory," *Space Sci. Rev.* **218**, 43 (2022).
17. P. Hartogh et al., "Direct detection of the Enceladus water torus with Herschel," *Astron. Astrophys.* **532**, L2 (2011).
18. D. C. Lis et al., "A Herschel study of D/H in water in the Jupiter-family comet 45P/Honda-Mrkos-Pajdušáková and prospects for D/H measurements with CCAT," *Astrophys. J. Lett.* **774**, L3 (2013).
19. D. Bockelée-Morvan et al., "Herschel measurements of the D/H and 16O/18O ratios in water in the Oort-Cloud comet C/2009 P1 (Garradd)," *Astron. Astrophys.* **544**, L15 (2012).
20. D. C. Lis et al., "Terrestrial deuterium-to-hydrogen ratio in water in hyperactive comets," *Astron. Astrophys.* **625**, L5 (2019).
21. S. S. Jensen et al., "ALMA observations of water deuteration: a physical diagnostic of the formation of protostars," *Astron. Astrophys.* **631**, A25 (2019).
22. N. Biver et al., "Isotopic ratios of H, C, N, O, and S in comets C/2012 F6 (Lemmon) and C/2014 Q2 (Lovejoy)," *Astron. Astrophys.* **589**, A78 (2016).
23. G. L. Villanueva et al., "A sensitive search for deuterated water in comet 8p/Tuttle," *Astrophys. J. Lett.* **690**, L5–L9 (2009).
24. L. Paganini et al., "Ground-based detection of deuterated water in comet C/2014 Q2 (Lovejoy) at IR wavelengths," *Astrophys. J. Lett.* **836**, L25 (2017).
25. A. Coutens et al., "A study of deuterated water in the low-mass protostar IRAS 16293-2422," *Astron. Astrophys.* **539**, A132 (2012).
26. A. Coutens et al., "Deuterated water in the solar-type protostars NGC 1333 IRAS 4A and IRAS 4B," *Astron. Astrophys.* **560**, A39 (2013).
27. A. Coutens et al., "Water deuterium fractionation in the high-mass star-forming region G34.26+0.15 based on Herschel/HIFI data," *Mon. Not. R. Astron. Soc.* **445**, 1299–1313 (2014).
28. M. V. Persson et al., "The deuterium fractionation of water on solar-system scales in deeply-embedded low-mass protostars," *Astron. Astrophys.* **563**, A74 (2014).
29. K. S. Wang, F. F. S. van der Tak, and M. R. Hogerheijde, "Kinematics of the inner thousand AU region around the young massive star AFGL 2591-VLA3: a massive disk candidate?" *Astron. Astrophys.* **543**, A22 (2012).
30. M. Emprechtinger et al., "The abundance, ortho/para ratio, and deuteration of water in the high-mass star-forming region NGC 6334 I," *Astrophys. J.* **765**, 61 (2013).
31. F. F. S. van der Tak et al., "Water in the envelopes and disks around young high-mass stars," *Astron. Astrophys.* **447**, 1011–1025 (2006).
32. F. P. Helmich, E. F. van Dishoeck, and D. J. Jansen, "The excitation and abundance of HDO toward W3(OH)/(H_2O)," *Astron. Astrophys.* **313**, 657–663 (1996).
33. E. F. van Dishoeck et al., "Water in star-forming regions: physics and chemistry from clouds to disks as probed by Herschel spectroscopy," *Astron. Astrophys.* **648**, A24 (2021).
34. L. Bonal et al., "Hydrogen isotopic composition of the water in CR chondrites," *Geochim. Cosmochem. Acta* **106**, 111–133 (2013).
35. L. Yang, F. J. Ciesla, and C. M. O. D. Alexander, "The D/H ratio of water in the solar nebula during its formation and evolution," *Icarus* **226**, 256–267 (2013).
36. E. Jacquet and F. Robert, "Water transport in protoplanetary disks and the hydrogen isotopic composition of chondrites," *Icarus* **223**, 722–732 (2013).
37. E. L. Gibb et al., "An infrared search for HDO in comet D/2012 S1 (ISON) and implications for iSHELL," *Astrophys. J.* **816**, 101 (2016).
38. N. Biver, R. Moreno, and D. Bockelée-Morvan, "HDO in comet 46p/Wirtanen from ALMA observations," (2024). In prep.
39. P. Eberhardt et al., "The D/H ratio in water from comet P/Halley," *Astron. Astrophys.* **187**, 435 (1987).
40. K. Altwegg et al., "67P/Churyumov-Gerasimenko, a Jupiter family comet with a high D/H ratio," *Science* **347**, 1261952 (2015).
41. N. Biver et al., "Comets iii," (2024). In press.
42. D. Bockelée-Morvan and N. Biver, "The composition of cometary ices," *Philos. Trans. R. Soc. Lond. Ser. A* **375**, 20160252 (2017).
43. C. J. Hansen et al., "Enceladus' water vapor plume," *Science* **311**, 1422–1425 (2006).
44. C. C. Porco et al., "Cassini observes the active south pole of Enceladus," *Science* **311**, 1393–1401 (2006).

45. J. H. Waite et al., "Cassini ion and neutral mass spectrometer: Enceladus plume composition and structure," *Science* **311**, 1419–1422 (2006).
46. A. Verbiscer et al., "Enceladus: cosmic graffiti artist caught in the act," *Science* **315**, 815 (2007).
47. A. R. Hendrix, C. J. Hansen, and G. M. Holsclaw, "The ultraviolet reflectance of Enceladus: implications for surface composition," *Icarus* **206**, 608–617 (2010).
48. M. M. Hedman and M. Young, "Evidence that a novel type of satellite wake might exist in Saturn's E ring," *Planet. Sci. J.* **2**, 127 (2021).
49. P. Hartogh et al., "Ocean-like water in the Jupiter-family comet 103P/Hartley 2," *Nature* **478**, 218–220 (2011).
50. T. Cavalié et al., "Herschel map of Saturn's stratospheric water, delivered by the plumes of Enceladus," *Astron. Astrophys.* **630**, A87 (2019).
51. G. L. Villanueva et al., "JWST molecular mapping and characterization of Enceladus' water plume feeding its torus," *Nat. Astron.* **7**, 1056–1062 (2023).
52. C. Plainaki et al., "Towards a global unified model of Europa's tenuous atmosphere," *Space Sci. Rev.* **214**, 40 (2018).
53. V. I. Shematovich et al., "Surface-bounded atmosphere of Europa," *Icarus* **173**, 480–498 (2005).
54. M. L. Marconi, "A kinetic model of Ganymede's atmosphere," *Icarus* **190**, 155–174 (2007).
55. M.-C. Liang et al., "Atmosphere of Callisto," *J. Geophys. Res.-Planets* **110**, E02003 (2005).
56. L. Roth et al., "Transient water vapor at Europa's south pole," *Science* **343**, 171–174 (2014).
57. L. Paganini et al., "A measurement of water vapour amid a largely quiescent environment on Europa," *Nat. Astron.* **4**, 266–272 (2020).
58. O. Grasset et al., "JUpiter ICy moons explorer (JUICE): an ESA mission to orbit Ganymede and to characterise the Jupiter system," *Plan. Space Sci.* **78**, 1–21 (2013).
59. P. Hartogh and Y. A. Ilyushin, "A passive low frequency instrument for radio wave sounding the subsurface oceans of the Jovian icy moons: an instrument concept," *Plan. Space Sci.* **130**, 30–39 (2016).
60. S. M. Howell and R. T. Pappalardo, "NASA's Europa Clipper—a mission to a potentially habitable ocean world," *Nat. Commun.* **11**, 1311 (2020).
61. R. Moreno et al., "The abundance, vertical distribution and origin of H_2O in Titan's atmosphere: Herschel observations and photochemical modelling," *Icarus* **221**, 753–767 (2012).
62. L. M. Lara et al., "A time-dependent photochemical model for Titan's atmosphere and the origin of H_2O," *Astron. Astrophys.* **566**, A143 (2014).
63. M. Dobrijevic et al., "Coupling of oxygen, nitrogen, and hydrocarbon species in the photochemistry of Titan's atmosphere," *Icarus* **228**, 324–346 (2014).
64. E. Lellouch et al., "The origin of water vapor and carbon dioxide in Jupiter's stratosphere," *Icarus* **159**, 112–131 (2002).
65. T. Cavalié et al., "Spatial distribution of water in the stratosphere of Jupiter from Herschel HIFI and PACS observations," *Astron. Astrophys.* **553**, A21 (2013).
66. B. Benmahi et al., "Monitoring of the evolution of H_2O vapor in the stratosphere of Jupiter over an 18-yr period with the Odin space telescope," *Astron. Astrophys.* **641**, A140 (2020).
67. N. A. Teanby et al., "Uranus's and Neptune's stratospheric water abundance and vertical profile from Herschel-HIFI," *Planet. Sci. J.* **3**, 96 (2022).
68. M. Küppers et al., "Localized sources of water vapour on the dwarf planet (1) Ceres," *Nature* **505**, 525–527 (2014).
69. E. Lellouch et al., "The deuterium abundance in Jupiter and Saturn from ISO-SWS observations," *Astron. Astrophys.* **370**, 610–622 (2001).
70. H. Feuchtgruber et al., "The D/H ratio in the atmospheres of Uranus and Neptune from Herschel-PACS observations," *Astron. Astrophys.* **551**, A126 (2013).
71. T. Cavalié et al., "Thermochemistry and vertical mixing in the tropospheres of Uranus and Neptune: how convection inhibition can affect the derivation of deep oxygen abundances," *Icarus* **291**, 1–16 (2017).
72. O. Venot et al., "New chemical scheme for giant planet thermochemistry. Update of the methanol chemistry and new reduced chemical scheme," *Astron. Astrophys.* **634**, A78 (2020).
73. E. Lellouch et al., "First results of Herschel-PACS observations of Neptune," *Astron. Astrophys.* **518**, L152 (2010).
74. J. D. R. Pierel et al., "D/H ratios on Saturn and Jupiter from Cassini CIRS," *Astron. J.* **154**, 178 (2017).
75. C. M. Anderson, M. S. Ugelow, and A. Tielens, "Refractive indices of amorphous and crystalline water ice films," In prep (2024).
76. I. Kamp et al., "The formation of planetary systems with SPICA," *Publ. Astron. Soc. Australia* **38**, e055 (2021).
77. M. M. Hedman et al., "Spectral observations of the Enceladus plume with Cassini-VIMS," *Astrophys. J.* **693**, 1749–1762 (2009).

78. B. Schmitt, J. M. Greenberg, and R. J. A. Grim, "The temperature dependence of the CO infrared band strength in CO: H_2O ices," *Astrophys. J. Lett.* **340**, L33 (1989).
79. W. M. Grundy and L. A. Young, "Near-infrared spectral monitoring of Triton with IRTF/SpeX I: establishing a baseline for rotational variability," *Icarus* **172**, 455–465 (2004).
80. A. Bieler et al., "Abundant molecular oxygen in the coma of comet 67P/Churyumov-Gerasimenko," *Nature* **526**, 678–681 (2015).
81. D. Laufer, A. Bar-Nun, and A. Ninio Greenberg, "Trapping mechanism of O_2 in water ice as first measured by Rosetta spacecraft," *Mon. Not. R. Astron. Soc.* **469**, S818–S823 (2017).
82. W. M. Grundy et al., "Surface compositions across Pluto and Charon," *Science* **351**, aad9189 (2016).
83. W. M. Grundy and U. Fink, "The absorption coefficient of the liquid N_2 2.15-μm band and application to triton," *Icarus* **93**, 169–173 (1991).
84. M. Bernstein, "Water ice on comets and satellites," in *Laboratory Astrophysics and Space Research*, P. Ehrenfreund et al., Eds., Astrophysics and Space Science Library, Vol. **236**, pp. 105–120, Springer (1998).
85. M. S. Gudipati and P. D. Cooper, "Chemistry in water ices: from fundamentals to planetary applications," in *Astrophysics and Space Science Library*, M. S. Gudipati and J. Castillo-Rogez, Eds., Astrophysics and Space Science Library, Vol. **356**, p. 503, Springer (2013).
86. W. M. Grundy et al., "Near-infrared spectral monitoring of Pluto's ices: spatial distribution and secular evolution," *Icarus* **223**, 710–721 (2013).
87. I. Wong et al., "The complex surface and atmospheric properties of Triton revealed by JWST/NIRSpec," *Bull. Amer. Astron. Soc.* **55**, 401.08 (2023).
88. E. Mazzotta Epifani et al., "The dust coma of the active centaur p/2004 a1 (loneos): a co-driven environment?" *Astron. Astrophys.* **460**(3), 935–944 (2006).
89. K. Wierzchos, M. Womack, and G. Sarid, "Carbon monoxide in the distantly active centaur (60558) 174P/Echeclus at 6 Au," *Astron. J.* **153**, 230 (2017).
90. F. Kemper, W. J. Vriend, and A. G. G. M. Tielens, "The absence of crystalline silicates in the diffuse interstellar medium," *Astrophys. J.* **609**, 826–837 (2004).
91. K. Malfait et al., "The ISO spectrum of the young star HD 142527," *Astron. Astrophys.* **345**, 181–186 (1999).
92. J. Kessler-Silacci et al., "c2d *Spitzer* IRS spectra of disks around T Tauri Stars. I. Silicate emission and grain growth," *Astrophys. J.* **639**, 275–291 (2006).
93. J. Crovisier et al., "The spectrum of comet Hale-Bopp (C/1995 O1) observed with the infrared space observatory at 2.9 astronomical units from the sun," *Science* **275**, 1904–1907 (1997).
94. D. Brownlee, "Comets and the early solar system," *Phys. Today* **61**, 30 (2008).
95. W. T. Reach et al., "Explosion of Comet 17P/Holmes as revealed by the *Spitzer* Space Telescope," *Icarus* **208**, 276–292 (2010).
96. D. H. Wooden, H. A. Ishii, and M. E. Zolensky, "Cometary dust: the diversity of primitive refractory grains," *Philos. Trans. R. Soc. Lond. Ser. A* **375**, 20160260 (2017).
97. L. W. Esposito et al., "Sulfur dioxide at the Venus cloud tops, 1978–1986," *J. Geophys. Res.* **93**, 5267–5276 (1988).
98. E. Marcq et al., "Variations of sulphur dioxide at the cloud top of Venus's dynamic atmosphere," *Nat. Geosci.* **6**, 25–28 (2013).
99. F. P. Mills and M. Allen, "A review of selected issues concerning the chemistry in Venus' middle atmosphere," *Plan. Space Sci.* **55**, 1729–1740 (2007).
100. V. A. Krasnopolsky, "A photochemical model for the Venus atmosphere at 47-112 km," *Icarus* **218**, 230–246 (2012).
101. A. C. Vandaele et al., "Sulfur dioxide in the Venus atmosphere: I. Vertical distribution and variability," *Icarus* **295**, 16–33 (2017).
102. J. S. Greaves et al., "Phosphine gas in the cloud decks of Venus," *Nat. Astron.* **5**, 655–664 (2020).
103. M. A. Thompson, "The statistical reliability of 267-GHz JCMT observations of Venus: no significant evidence for phosphine absorption," *Mon. Not. R. Astron. Soc.* **501**, L18–L22 (2021).
104. G. L. Villanueva et al., "No evidence of phosphine in the atmosphere of Venus from independent analyses," *Nat. Astron.* **5**(7), 631–635 (2021).
105. A. B. Akins et al., "Complications in the ALMA detection of phosphine at Venus," *Astrophys. J. Lett.* **907**, L27 (2021).
106. T. Encrenaz et al., "A stringent upper limit of the PH3 abundance at the cloud top of Venus," *Astron. Astrophys.* **643**, L5 (2020).
107. L. Trompet et al., "Phosphine in Venus' atmosphere: detection attempts and upper limits above the cloud top assessed from the SOIR/VEx spectra," *Astron. Astrophys.* **645**, L4 (2021).
108. D. Bockelée-Morvan et al., "Searches for HCl and HF in comets 103P/Hartley 2 and C/2009 P1 (Garradd) with the Herschel Space Observatory," *Astron. Astrophys.* **562**, A5 (2014).

109. S. Faggi et al., "Strongly depleted methanol and hypervolatiles in comet C/2021 A1 (Leonard): signatures of interstellar chemistry?" *Planet. Sci. J.* **4**, 8 (2023).
110. F. Dhooghe et al., "Halogens as tracers of protosolar nebula material in comet 67P/Churyumov-Gerasimenko," *Mon. Not. R. Astron. Soc.* **472**, 1336–1345 (2017).

Carrie M. Anderson is a research scientist at NASA Goddard Space Flight Center (GSFC). She received her BS degree in physics from Arizona State University in 2000 and her MS and PhD degrees in astronomy from New Mexico State University in 2003 and 2006, respectively. She is the author of more than 45 papers in refereed journals and has written one book chapter. Her research focuses on the remote sensing of planetary atmospheres, primarily in the areas of thermal structure and composition, using space- and ground-based data, in the visible, near-IR, mid-IR, far-IR, and submillimeter spectral regions. Her research also includes laboratory transmission spectroscopy measurements of ice films in a high-vacuum cryo chamber located in her Spectroscopy for Planetary ICes Environments (SPICE) laboratory at NASA GSFC.

Nicolas Biver holds a permanent research position at the French Center for Scientific Research (CNRS) at Paris Observatory. He received his MS degree in physics from Paris-Cité University in 1993, after graduating from the engineering high school "Ecole Centrale" in 1992. He defended his PhD in astrophysics on the observation and modeling of rotational lines of molecules in cometary comae from the Paris-Cité University in 1997. He is the author of more than 100 journal papers (25 as first author) and has written a book chapter on cometary chemistry (in Comets III, to be published in 2024). His current research interests include the molecular and isotopic composition of cometary volatiles and observations of solar system objects in the millimeter to submillimeter range.

Gordon L. Bjoraker is a research scientist at the NASA GSFC. He received his BS degree in physics and astronomy from the University of Wisconsin in 1978 and his PhD in planetary science from the University of Arizona in 1985. He is the author of more than 90 journal papers. His research focuses on the remote sensing of planetary atmospheres, primarily in the areas of gas composition and cloud structure, using space- and ground-based data, in the near-IR, mid-IR, far-IR, and submillimeter spectral regions.

Thibault Cavalié is a permanent research scientist for the CNRS at the Laboratoire d'Astrophysique de Bordeaux. He received his BS and MS degrees in physics from the University of Bordeaux in 2003 and 2005, respectively, and his PhD in astrophysics on the observation of oxygen species in the millimeter and submillimeter in planetary atmospheres in preparation for Herschel and ALMA from the University of Bordeaux in 2008. He is the author of more than 60 journal papers. His current research interests include mid-IR, far-IR, and submillimeter spectroscopy using space- and ground-based data as well as chemical modeling of giant planet atmospheres to understand their formation and evolution.

Gordon Chin is a research scientist at NASA GSFC. He received his BA degree in physics from Columbia College in 1970 and his MA, MPhil, and PhD degrees in physics from Columbia University in 1972, 1974, and 1977, respectively. He is the author of more than 50 refereed journal papers. His current research interests include the development of submillimeter planetary flight spectrometers targeting planetary atmospheres, the lunar exosphere, and ocean world plume environments in the solar system.

Michael A. DiSanti is a research scientist at NASA GSFC. He received his BS and MS degrees in physics from the University of New Mexico in 1978 and 1980, respectively, and his PhD in physics from the University of Arizona in 1989. He has co-authored more than 50 journal papers and two book chapters. His current research interests include the composition of cometary ices and their relationship to solar system formation.

Paul Hartogh leads the atmospheric science group in the planetary department of the Max Planck Institute for Solar System Research (MPS). He received his diploma and PhD in physics from the University of Göttingen in 1985 and 1989, respectively. He is the author of more than 250 journal papers and has written more than 10 book chapters. His current research interests include atmospheres in the solar system and as the principal investigator of the Submillimeter

Wave Instrument (SWI) on the JUpiter ICy moons Explorer (JUICE) with a focus on the Jupiter system.

Nathan X. Roth is an assistant professor at American University, conducting his research off-site at the NASA GSFC. He received his BS and MS degrees in physics and astrophysics from the University of Missouri–St. Louis in 2014 and 2016, respectively, and his PhD in physics from the Missouri University of Science & Technology in 2019. He is the author of more than 40 journal papers and has written one book chapter. His current research interests include radio and infrared spectroscopy of solar system objects, including comets and asteroids, and applications to planetary defense.

Alexander Tielens is a professor of astronomy in the Astronomy Department of the University of Maryland, College Park. He received his MS and PhD degrees in astronomy from Leiden University in 1982. He has authored over 500 papers in refereed journals and has written two textbooks on the interstellar medium. His scientific interests center on the physics and chemistry of the interstellar medium, in particular, in regions of star and planet formation.

Christopher K. Walker is a professor of astronomy, optical sciences, electrical and computer engineering, aerospace and mechanical engineering, and applied mathematics at the University of Arizona. He received his MSEE degree from Clemson University (1980), his MSEE degree from Ohio State University (1981), and his PhD in Astronomy from the University of Arizona (1988). He was an employee at TRW Aerospace and the Jet Propulsion Laboratory, was a Millikan Fellow in Physics at Caltech, and has been a faculty member at the University of Arizona since 1991, where he has served to advance the field of terahertz astronomy. He has supervised 16 PhD students, led numerous NASA and NSF projects, authored/coauthored 130+ papers, and published two textbooks: *Terahertz Astronomy* and *Investigating Life in the Universe*.